Von Herzen, R. P., Robinson, P. T., et al., 1991
Proceedings of the Ocean Drilling Program, Scientific Results, Vol. 118

8. METAMORPHIC STRATIGRAPHY OF HOLE 735B[1]

Debra Stakes,[2] Catherine Mével,[3] Mathilde Cannat,[3] and Teresa Chaput[2]

ABSTRACT

Gabbroic rocks and their late differentiates recovered at Site 735 represent 500 m of oceanic layer 3. The original cooling of a mid-ocean ridge magma chamber, its penetration by ductile shear zones and late intrusives, and the subsequent penetration of seawater through a network of cracks and into highly permeable magmatic hydrofracture horizons are recorded in the metamorphic stratigraphy of the core. Ductile shear zones are characterized by extensive dynamic recrystallization of primary phases, beginning in the granulite facies and continuing into the lower amphibolite facies. Increasing availability of seawater during dynamic recrystallization is reflected in depletions in ^{18}O, increasing abundance of amphibole of variable composition and metamorphic plagioclase of intermediate composition, and more complete coronitic or pseudomorphous static replacement of magmatic minerals. Downcore correlation of synkinematic assemblages, bulk-rock oxygen isotopic compositions, and vein abundance suggest that seawater is introduced into the crust by way of small cracks and veins that mark the end of the ductile phase of deformation. This "deformation-enhanced" metamorphism dominates the upper 180 and the lower 100 m of the core.

In the lower 300 m of the core, mineral assemblages of greenschist and zeolite facies are abundant within or adjacent to brecciated zones. Leucocratic veins found in these zones and adjacent host rock contain diopside, sodic plagioclase, epidote, chlorite, analcime, thomsonite, natrolite, albite, quartz, actinolite, sphene, brookite, and sulfides. The presence of zircon, Cl-apatite, sodic plagioclase, sulfides, and diopside in leucocratic veins having local magmatic textures suggests that some of the veins originated from late magmas or from hydrothermal fluids exsolved from such magmas that were subsequently replaced by (seawater-derived) hydrothermal assemblages. The frequent association of these late magmatic intrusive rocks within the brecciated zones suggests that they are both artifacts of magmatic hydrofracture. Such catastrophic fracture and hydrothermal circulation could produce episodic venting of hydrothermal fluids as well as the incorporation of a magmatically derived hydrothermal component. The enhanced permeability of the brecciated zones produced lower temperature assemblages because of larger volumes of seawater that penetrated the crust. The last fractures were sealed either by these hydrothermal minerals or by late carbonate-smectite veins, resulting in the observed low permeability of the core.

INTRODUCTION

Plutonic rocks probably are a major constituent of the oceanic crust because they are presumed to form most of the seismically defined layer 3. Samples collected by dredging or with submersibles have proved heterogeneous in terms of their magmatic type (varying from ultramafic cumulates to plagiogranites) as well as their metamorphic imprint (see for instance, Fox and Stroup, 1981). Detailed petrologic studies of oceanic gabbros have demonstrated that metamorphic recrystallization is related either to deformation and/or interaction with seawater during the progressive cooling of the gabbroic sequence (Bonatti et al., 1975; Helmstaedt and Allen, 1977; Ito and Anderson, 1983; Prichard and Cann, 1983; Honnorez et al., 1984; Mevel, 1987, 1988). The influence of deformation on seawater penetration, and therefore metamorphic crystallization in particular, has been stressed (Ito and Anderson, 1983; Vanko and Batiza, 1982; Batiza and Vanko, 1985; Mevel, 1988).

Identifying metamorphic reactions in oceanic gabbros is of great interest because the thermal and tectonic evolution of the lower crust is recorded in these metamorphic minerals. However, samples dredged or collected by submersible lack the detailed field relationships that are essential for understanding such heterogeneous material. The suite of gabbroic rocks drilled on the Southwest Indian Ridge (SWIR) during Leg 118 is a unique data set for addressing the problem of subsolidus evolution of oceanic lower crust. Because of the unprecedented recovery (87%), the core permits detailed study of the nature and distribution of metamorphic crystallization, and its relationship to deformation. The results of this study provide a model for the initial penetration and circulation of seawater into the lower crust.

Hole 735B was drilled during Leg 118 in 1987. The site was placed in the center of a 9- x 4-km horst block 90 km south of the SWIR. The center of the block was selected for drilling to avoid intercepting the relatively young faults that bound the horst. This block (a 700-m-deep wave-cut terrace) is the shallowest portion of the transverse ridge that parallels the Atlantis II (AII) Fracture Zone. The crust comprising the block was formed at the SWIR about 12 m.y. ago, an age based on the magnetic anomalies and deduced spreading rate (Dick et al., 1990a) and verified by zircon lead (Pb) isotopic dating (11.3 Ma, J. Mattinson, pers. comm., 1989). During 17 days of drilling, scientists penetrated 500.3 m into gabbro representing oceanic layer 3 for the SWIR adjacent to the AII transform. The 436 m of recovered core comprises gabbro of variable primary composition, from olivine-rich to Fe-Ti oxide-rich compositions, as well as small volumes of late magmatic intrusive rocks (LMI), including a trondhjemite and zircon-bearing felsic intrusions. Approximately 50% of the core has been affected by metamorphism, including dynamic recrystallization of magmatic phases, joined by increasing abundances of amphibole, static recrystallization and hydrous replacement of primary phases, hydrothermal mineralization,

---

[1] Von Herzen, R, Robinson, P. T., et al., 1991. *Proc. ODP, Sci. Results*, 118: College Station, TX (Ocean Drilling Program).

[2] Department of Geological Sciences, University of South Carolina, Columbia, SC 29208, U.S.A.

[3] Laboratoire de Pétrologie, Université de Brétagne Occidentale, 6 Ave le Gorgeu, 29287 Brest Cedex, France.

and alteration by fluids associated with the LMI. The history of fluid-rock interactions and their associated mineral assemblages is complex and similar to what has been observed for continental intrusions (e.g., Norton et al., 1984; Bird et al., 1986, 1988), except that the fluid in this system is predominately seawater.

The purpose of this study is to characterize the sequence of metamorphic events and the resulting stratigraphic distribution of secondary phases. Our results suggest that the major ductile faults that crosscut the core served as conduits for seawater to penetrate cooling oceanic crust at temperatures that were initially near 700°C. Deformation mechanisms and tectonic evolution are discussed in two companion chapters (Cannat, this volume; Cannat et al., this volume). Composition of the fluids circulating during metamorphism is discussed in a third chapter (Vanko and Stakes, this volume).

ANALYTICAL METHODS

Mineral Chemistry and Petrography

A set of more than 200 polished thin sections was used for petrographic descriptions and microprobe analyses. These detailed petrographic analyses supplement the reconnaissance analyses performed on board the *JOIDES Resolution* by the shipboard scientists. The entire sample number for each specimen can be designated as 118-735B-XX-Y, Pc. P (Z-Z cm), where XX-Y are the core and section number, P is the piece number, and Z-Z is the interval, as measured from the top of the section. Microprobe analyses were performed on a subset of 30 samples using the Cameca SX-50 electron microprobe facilities at the University of South Carolina, the Camebax microprobe at the Université de Paris VI (Camparis), and the Université de Brétagne Occidentale (Microsorde de l'Ouest). A structural log (Fig. 1) was produced by one of the authors (MC) from the shipboard core descriptions.

Oxygen Isotope Analyses

Oxygen isotope analyses were performed at the University of South Carolina, using standard techniques. Samples were reacted with ClF_3 in nickel tubes to extract the oxygen, which was subsequently converted to CO_2 by reaction with a glowing carbon rod. Isotopic analyses were performed on a VG 602 Micromass mass spectrometer. All analyses were performed in replicate with either NBS-28 or Ottawa sand as standards, with an accuracy of ± 0.3 per mil (‰).

Results of oxygen isotopic analyses are presented in Table 1 and Figure 1. Results are reported in standard δ-notation, where an increase in δ (δ) represents a relative enrichment in the heavier isotope compared to standard mean ocean water (SMOW = 0‰). Two types of samples were analyzed. The first type was homogeneous whole-rock powders. A total of 94 such powders were prepared on board the *JOIDES Resolution* for X-ray fluorescence (XRF) analyses. During the cruise, the upper section of the core was more heavily sampled for XRF analyses. Samples were selected from the freshest and most altered portions of each recovered section. The lower one-half of the core was sampled much less thoroughly because of time constraints, and the shipboard suite of samples was selected from only the freshest-appearing portion of each section. Additional whole-rock powders were prepared for the land-based isotopic study to supplement these shipboard samples, especially to include the more intensely altered samples from the last 20 cores. Most samples are a "bulk" composition; i.e., a homogeneous powder derived from 2 to 5 g of what is typically a coarsely heterogeneous altered rock. These may include heavily fractured and veined material. Splits were analyzed for oxygen isotopes (1) to assess the general effects of metamorphism on the core, (2) to determine whether oxygen isotopic composition and bulk chemistry show any consistent variation, and (3) to illuminate the nature of the fluid responsible for metamorphism.

The second sample type for which oxygen isotopes were determined was samples having discrete veins. In these samples, the vein material and host matrix were analyzed separately and the whole-rock powder or separated mineral phases of the host was designated matrix (= M), whereas the vein minerals have been reported separately and designated vein (= V). Mineral separates were produced by a combination of magnetic separation, followed by handpicking. Separates from unveined or pervasively veined and altered material lack the M/V designation. Detailed petrography and microprobe analyses show that feldspars within the pervasively altered regions may be complexly zoned or veined with sodic plagioclase, analcime, prehnite, or thomsonite. Where calcic and sodic plagioclase could be optically distinguished, they were analyzed separately. Estimated temperatures (based on the oxygen isotopic composition of separates of plagioclase and diopside) are reported in conjunction with fluid inclusion data in Vanko and Stakes (this volume.)

MAGMATIC STRATIGRAPHY

The core was divided into six lithologic units by the shipboard party on the basis of mineralogical and structural discontinuities. A subsequent, land-based redescription of the lithology suggests that the units are much more complex than the original stratigraphy, with 493 distinct lithologic boundaries. The revised lithostratigraphy is included in this volume (Dick et al., this volume, b) and is summarized here and in Figure 1. The six units of the revised lithostratigraphy are Subunit IA = deformed gabbro norite (Cores 118-735B-1D-1 to 118-735B-7D-1; 0–28.0 mbsf); Subunit IB = mixed gabbro norite and olivine gabbro (Cores 118-735B-7D-1 to 118-735B-10R-1; 28.0–37.5 mbsf); Unit II = olivine gabbro with intervals of synkinematic oxide and oxide-olivine gabbro and intrusive microgabbro and olivine gabbro (Cores 118-735B-10R-1 to 118-735B-35R-6; 37.5–170.2 mbsf); Subunit IIIA = disseminated oxide olivine and olivine gabbro (Cores 118-735B-35R-6 to 118-735B-37R-3; 170.2–180.1 mbsf); Subunit IIIB = massive disseminated oxide olivine gabbro (Cores 118-735B-37R-3 to 118-735B-43R-3, 180.1–209.5 mbsf); Subunit IIIC = disseminated oxide olivine and olivine gabbro (Cores 118-735B-43R-3 to 118-735B-46R-3, 209.5–223.6 mbsf); Unit IV = massive oxide olivine gabbro (Cores 118-735B-46R-3 to 118-735B-56R-3, 223.6–274.1 mbsf); Unit V = massive olivine gabbro (Cores 118-735B-56R-3 to 118-735B-73R-7, 274.1–382.4 mbsf); Subunit VIA = compound olivine gabbro with minor intervals of intrusive oxide microgabbro norite and olivine microgabbro and synkinematic oxide and oxide-olivine gabbro (Cores 118-735B-77R-1 to 118-735B-79R-4, 382.4–404.0 mbsf); Subunit VIB = compound olivine, oxide-olivine, and disseminated oxide-olivine gabbro with minor intrusive olivine and oxide-olivine microgabbro (Cores 118-735B-79R-4 to 118-735B-81R-1, 404.0–419.3 mbsf); Subunit VIC = compound troctolitic and olivine gabbro with minor synkinematic oxide-olivine gabbro and oxide-olivine microgabbro and intrusive troctolite and troctolitic microgabbro (Cores 118-735B-81R-1 to 118-735B-88R-1, 419.3–433.8 mbsf); Subunit VID = compound olivine and oxide-olivine and troctolitic gabbro with synkinematic disseminated-oxide-olivine and oxide gabbro (Cores 118-735B-88R-1 to 118-735B-87R-7, 433.8–500.1 mbsf).

Gabbros

Most of the core (61%) is chemically uniform, massive olivine gabbro with minor cryptic variations. The abundance of olivine varies from 1% to 20%, and its composition is magnesian (Fo_{74}). Plagioclase is moderately anorthitic (An_{58}) and clinopyroxene is magnesian ($Mg_{81.2}$). A small unit of gabbro norite occurs at the top of the section, and the bottom 80 m contains intercalated troctolitic gabbros and microgabbros. The olivine gabbro is relatively primitive in bulk rock composition, more primitive than the gabbronorites (with plagioclase = An_{40} and clinopyroxene = Mg_{70}) and microgabbros, but less magnesian and anorthitic than the troctolitic rocks (see Dick et al., 1990b Appendix II). The contacts between units vary from pegmatoidal patches to intrusive and are frequently sheared and deformed. Dick et al. (this volume, b) suggest that they record a continuous cycle of syndeformational magmatic activity.

Later Intrusive Units

The abundance of Fe-Ti oxide rich layers and of small intrusions of late leucocratic rocks was underestimated during the shipboard descriptions. The latter are particularly important because they seem to play a significant role in the distribution of metamorphic assemblages.

Ferrogabbros

One of several unanticipated features of the rocks recovered from Hole 735B was the presence of concentrations of ilmenite and magnetite. Many of these concentrations are associated with deformed zones, suggesting to the shipboard party that there may have been either a hydrothermal mechanism for the oxide distribution or a preferred localization of the deformation in oxide-rich intervals. Clearly, the oxide-rich gabbros have rheological properties favorable to strain localization: the best-developed mylonite zones are also those for which the matrix is predominately Fe-Ti oxide. Apparently, there is local redistribution of ilmenite during dynamic metamorphism, as oxides often fill the synkinematic microcracks in the pyroxene and plagioclase porphyroclasts. However, deformed and undeformed oxide concentrations can be found within a single section, suggesting that the oxide concentrations preceded the formation of the shear zones (see Cannat et al., this volume, for a more complete discussion). Dick et al. (b, this volume) conclude that the oxide concentrations are contemporaneous with deformation, a "syndeformation magmatic fractionation." Differentiation of oceanic gabbros leads to ferrogabbroic compositions extremely enriched in titanium and iron (Miyashiro and Shido, 1980; Prinz et al., 1976). Field relationships in ophiolitic gabbros show that these ferrogabbros often occur as centimetric to decimetric pockets or dykelets (pers. observation in the Chenaillet ophiolite, Western Alps, for example). We conclude that the oxide concentrations result from late magmatic, not hydrothermal processes. Within some zones, these may be subjected to deformation events and hydrothermally altered by circulation of fluids, but this does not indicate a hydrothermal origin for the initial concentrations. Bird et al. (1986) observed Fe-Ti-rich gabbro pegmatites and pyroxene-oxide veins in the Skaergaard Intrusion, which they related to the local redistribution of evolved magma. The Fe-oxides found in the Skaergaard are mixtures of Ti-magnetite and ilmenite, similar to the oxide-rich horizons described for the Hole 735B core. Estimated temperatures for the Skaergaard pyroxene-oxide veins of 900°C is consistent with a late magmatic origin.

Leucocratic Rocks (Including Trondhjemite)

Small quantities of late felsic intrusives were found at several zones in the core. The leucocratic rocks form small pockets or dykelets of centimetric size. These injections of late felsic melts characteristically intruded into brecciated zones. They have a distinctive texture characterized by euhedral sodic plagioclase laths (Pl. 1, Fig. 1) sometimes observed as nucleating on partially resorbed margins of preexisting calcic plagioclase. They are characterized by a distinct mineralogical assemblage, including the euhedral laths of sodic plagioclase or albite, scattered greenish clinopyroxene, small grains of zircon and possibly biotite, apatite, and sometimes quartz (Pl. 1, Fig. 2). The rare quartz contains secondary aqueous fluid inclusions, probably metamorphic in origin (Vanko and Stakes, this volume). These felsic intrusions have been interpreted as representing the latest product of magmatic differentiation, and we call them late magmatic intrusions (LMI). Dick et al. (this volume, b) considers them the silicic complement to the ferrogabbros. They are concentrated within the lower half of the core. The largest horizon is the trondhjemite intrusion in Cores 118-735B-53R through 118-735B-56R that contains partially resorbed xenoliths of gabbro, distinguished by euhedral sodic plagioclase mantling partially digested calcic plagioclase.

Because many of the phases in the late magmatic intrusives are similar to those in the hydrothermal breccias (discussed later), we use the texture (euhedral plagioclase, granophyres) and presence or absence of quartz or zircon to distinguish late magmatic and hydrothermal assemblages. In Figure 1, felsic or leucocratic veins (LCV) are plotted downcore without distinguishing a magmatic or hydrothermal origin. The stratigraphic relationship between these leucocratic veins and the appearance of zircon (ZR in Fig. 1) argues strongly for the participation of magmatic fluids, in at least the early stages of formation. These magmatic/hydrothermal assemblages are found as scattered deformed lenses in otherwise undeformed sections. An example of this can be seen in Core 118-735B-35R-2 (described below), in which a 1-cm deformation zone through an otherwise undeformed orthopyroxene-bearing gabbro contains a fine-grained assemblage of quartz, sodic plagioclase, actinolite, and diopside. A similar 1- to 2-cm-wide lens of quartz-albite-epidote-biotite occurs in Core 118-735B-35R-5, Pc. 4C.

DEFORMATION

Plastic Deformation

Textural Types

The "Textural Type" log (Fig. 1) shows the distribution of deformation intensities within the core. The categories of ductile deformation are as follows:

1. Type I = weakly deformed with no penetrative deformation and incipient recrystallization of plagioclase.
2. Type II = well-foliated, with limited dynamic recrystallization of plagioclase.
3. Type III = well-foliated with extensive dynamic recrystallization of plagioclase and size reduction of the mafic porphyroclasts (gneissic banding).
4. Type IV = extensive plagioclase recrystallization with millimeter-thick mylonite bands;
5. Type V = mylonitic.

Detailed descriptions of these textures and the mechanical aspects of their formation is given in Cannat et al. (this volume). The Textural Type log represents averages for each core, with intervals too small to plot individually, indicated by the shaded region. Approximately half of the core has been affected by some grade of dynamic recrystallization. Dick et al. (this volume, b) use a slightly different scale to assess deformation, but the resulting profile is almost identical to that produced on board the drill ship.

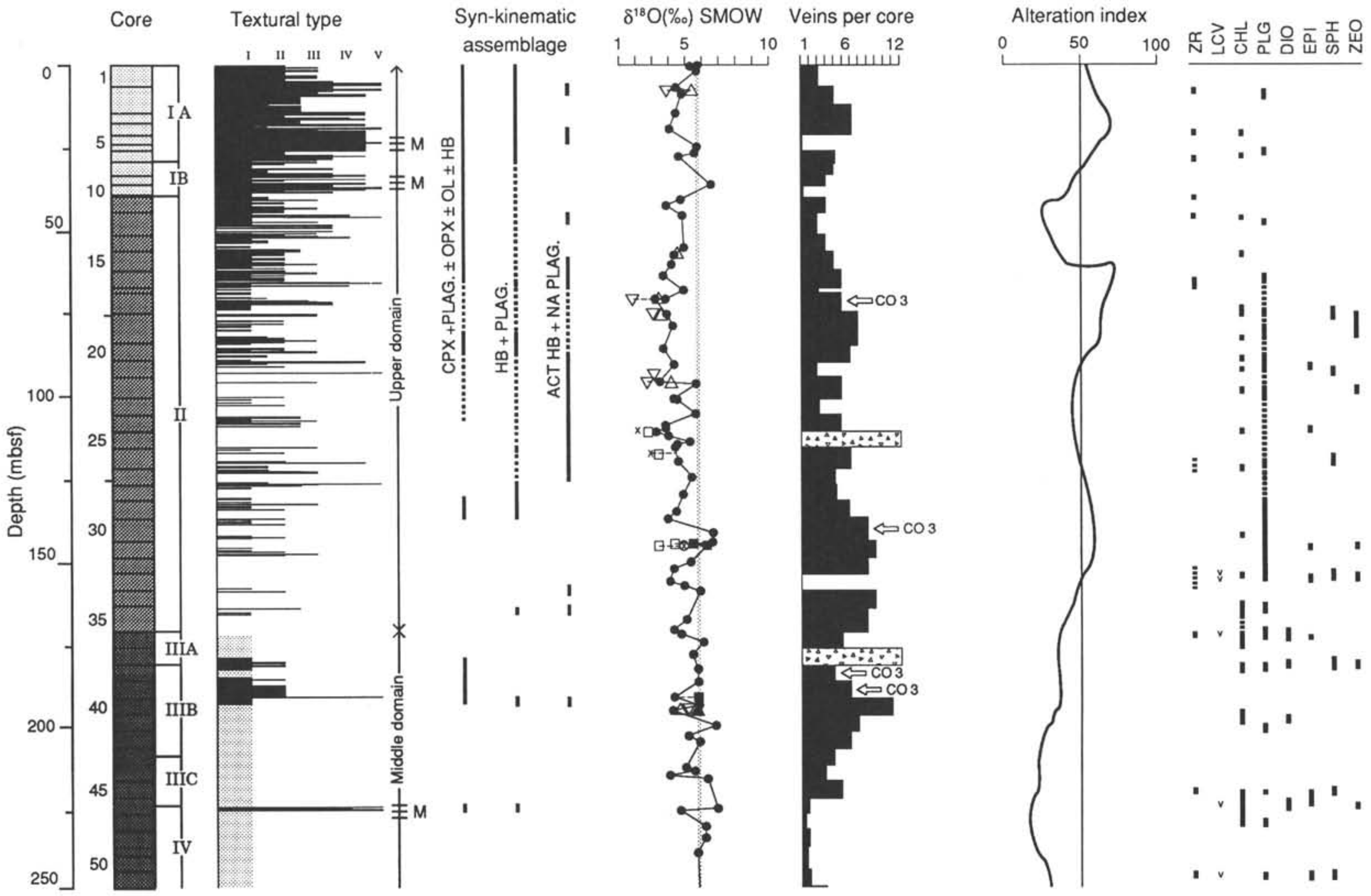
Core
Textural type
I II III IV V
Syn-kinematic assemblage
CPX +PLAG. ± OPX ± OL ± HB
HB + PLAG.
ACT HB + NA PLAG.
δ18O(‰) SMOW
1 5 10
Veins per core
1 6 12
CO 3
Alteration index
0 50 100
ZR
LCV
CHL
PLG
DIO
EPI
SPH
ZEO
Depth (mbsf)
0
50
100
150
200
250
1
5
10
15
20
25
30
35
40
45
50
I A
IB
II
IIIA
IIIB
IIIC
IV
M
Upper domain
Middle domain

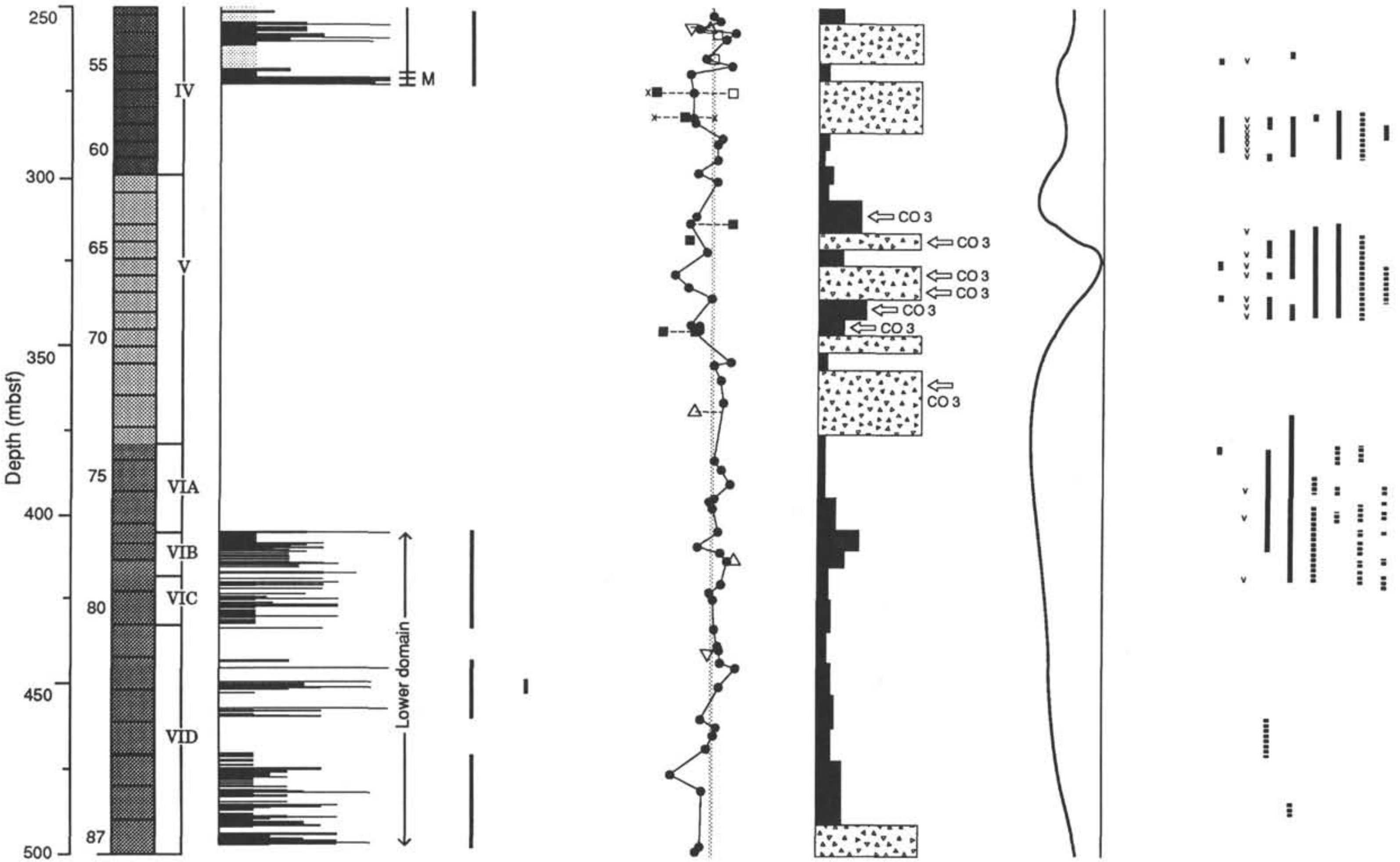

Figure 1. Metamorphic and deformation stratigraphy for Hole 735B. From left to right the columns represent (1) Depth and core number with shaded areas primary lithostratigraphy from Dick et al. (this volume): Unit I = gabbro norite; Unit II = compound olivine and oxide gabbro; Unit III = disseminated oxide-olivine gabbro; Unit IV = massive oxide olivine gabbro; Unit V = massive olivine gabbro; Unit VI = compound olivine, oxide and troctolitic gabbro; (2) Textural type as indicator of extent of synkinematic recrystallization: type I = weakly deformed with no penetrative deformation; type II = well-foliated with limited plagioclase recrystallization; type III = well-foliated with extensive plagioclase recrystallization and gneissic banding; type IV = gneissic banding interlayered with mylonitic bands; type V = mylonitic; structural domains are indicated as well as major mylonite zones (m); (3) synkinematic assemblages = secondary minerals that formed under plastic deformation; (4) profile of $\delta^{18}O$ vs. depth. Symbols on the oxygen isotope profile are as follows: filled circles = whole-rock powders; x in circle = matrix of vein; x = vein hornblende; filled box = vein plagioclase; x in square = vein clinopyroxene; open upside down triangle = whole-rock hornblende; open triangle = whole-rock plagioclase; open square = plagioclase from matrix of vein. Shaded bar represents average for fresh gabbroic rock; (5) histogram of the number of veins per core, with patterned intervals representing heavily veined brecciated horizons. Histogram includes all veins, dominantly hornblende-bearing to bottom of Core 118-735B-54R. Carbonate veins are indicated by arrows; (6) alteration index (= relative replacement [0%–100%] by coronitic and pseudomorphous assemblages) based on the replacement of pyroxene by amphibole; (7) stratigraphy of vein and replacement minerals in addition to amphibole and pseudomorphous assemblages.

Table 1. Oxygen isotope results.

Core, sect., interval (cm)	Code	Depth (mbsf)	W/R	PLAG	AMPH	DI	CPX
735B-1H-11, 90–92		0.9	5.7				
1D-1, 117–120	XRF	1.2	5.1				
1D-2, 91–94	XRF	2.4	5.6				
2D-1, 76–80	XRF	7.3	4.3				
2D-2, 36–39	VAN	8.4	Vein	4.8	4.0		
2D-2, 116–120	XRF	9.2	4.7				
3D-1, 46–49	XRF	15.0	4.1				
4D-2, 10–16	XRF	19.1	3.9				
6D-1, 71–74	XRF	24.7	5.7				
7D-1, 63–67	XRF	26.6	5.5				
7D-2, 1–5	XRF	27.5	4.4				
10R-1, 37–39				6.6	6.1		5.8
10R-1, 46–49	XRF	36.7	6.3		6.1		
12R-1, 118–123	XRF	40.6	4.5				
12R-2, 135–137	STA	42.2	3.6				
13R-1, 102–105	XRF	45.5	4.5				
14R-3, 136–141	XRF	55.1	5.0				
15R-1, 90–93	XRF	57.1	4.2	4.4			
15R-3, 92–96	XRF	60.1	4.2				
16R-1, 139–141	XRF	63.2	3.6				
17R-1, 22–27	XRF	67.2	4.8				
18R-2, 143–146	XRF	71.4	3.7				
18R-3, 5–8	STA	71.6	3.2	3.2	1.6		
18R-3, 37–40	XRF	71.9	3.1				
19R-1, 124–128	STA	75.9	3.8	3.4	2.9		
19R-3, 5–9	VAN	77.7					
19R-3, 73–75	XRF	78.3	4.0				
20R-2, 23–27	XRF	85.8	3.7				
21R-2, 53–56	XRF	90.7	4.3				
22R-1, 56–62	KEM				2.8		
22R-1, 142–147	XRF	95.5	3.3	3.9	3.0		
22R-2, 86–91	XRF	96.4	5.6				
22R-3, 112–115	VAN	98.2	Vein	4.0	3.6		
23R-2, 42–48	XRF	101.6	4.4				
23R-2, 66–73	XRF	101.8	4.5				
23R-4, 83–86	XRF	104.8	5.5				
24R-2, 47–51	STA	108.1	3.6				
24R-4, 1–6	XRF	109.8	3.6				
25R-1, 12–17	VAN	110.6	Ca-plg	4.9			
			Na-plg	2.4	1.9		
25R-1, 21–25	XRF	110.7	3.2				
25R-3, 43–48	XRF		3.8				
25R-3, 144–146	XRF	114.7	5.0				
26R-1, 131–134	XRF	116.8	4.5				
26R-2, 8–12	VAN	117.1		3.2	2.7		5.1
26R-4, 91–92	XRF	120.9	4.5				
27R-3, 73–81	XRF	125.2	5.4				
28R-3, 63–69	XRF	130.1	4.8				
29R-3, 124–130	XRF	135.6	4.3				
30R-1, 135–138	XRF	137.9	3.8				
30R-5, 110–115	XRF	143.5	6.5				
31R-2, 40–45	XRF	145.4	6.2				
31R-2, 77–81	XRF	145.8	4.6				
31R-2, 100–104	STA	146.1	4.1				
			Vein	5.3			
31R-3, 31–33	STA	146.7	3.6	3.5	5.3		
			Vein	5.5			
32R-3, 54–60	XRF	151.7	5.1				
32R-4, 43–49	XRF	152.5	4.3				
33R-3, 85–89	XRF	157.3	3.9				
33R-4, 27–29	XRF	158.1	4.6				
34R-2, 18–22	XRF	160.0	5.7				
35R-4, 43–46	XRF	168.3	4.8				
35R-6, 114–117	STA	171.9	4.3				5.4
36R-2, 98–102	XRF	173.5	4.5				
36R-4, 30–33	XRF	175.1	5.8				
37R-3, 80–82	XRF	179.6	5.3				
38R-2, 78–84	XRF	183.3	5.6				
39R-1, 145–157	XRF	187.5	5.7				
40R-2, 73–78	STA	192.2	4.2				
			Vein	6.4			
40R-4, 1–5	XRF	194.4	5.8				
41R-1, 42–50	STA	196.9	4.2	4.5	4.8		5.2
41R-4, 22–27	XRF	200.4	6.7				
42R-3, 9–14	XRF	204.0	5.0				
43R-1, 22–29	XRF	206.2	5.7				
44R-2, 6–8	XRF	213.1	4.8				
44R-3, 78–81	XRF	214.4	5.6				
44R-4, 41–49	STA	215.5	3.9				
45R-1, 48–54	XRF	216.5	6.3				
46R-3, 121–129	XRF	225.1	6.7				
46R-4, 109–113	XRF	226.5	4.6				
47R-4, 80–86	XRF	231.2	5.9				
48R-2, 109–113	XRF	233.4	6.0				
50R-2, 43–47	XRF	239.5	5.5				
52R-4, 88–94	XRF	252.9	5.7				
53R-1, 47–54	XRF	253.5	5.8				
53R-4, 5–15	STA	256.9	4.7	5.3	4.4		
53R-5, 40–43	XRF	258.5	7.0				
54R-1, 131–136	XRF	259.3	6.3				
55R-1, 59–69	STA	265.3	5.3	4.2	4.6		
55R-2, 101–105	XRF	267.5	6.7				
56R-1, 54–61	STA	270.7	4.3				
57R-2, 11–18	STA	276.4	4.4	4.0	1.8	5.2	
	STA		Vein	6.6	5.8		
58R-3, 8–16	STA	283.3	4.4				
			Vein	3.9	2.1	5.6	
58R-3, 107–114	XRF	284.3	4.5				
59R-4, 29–35	XRF	289.6	6.0				
60R-1, 80–83	XRF	291.3	5.9				
61R-1, 81–85	XRF	296.3	5.9				
61R-3, 48–58	STA	299.0	4.7				
62R-1, 92–94	XRF	301.4	5.9				
63R-5, 126–130	XRF	312.2	4.6				
63R-6, 94–98	VAN	313.4	Vein	6.7		4.4	
			Matrix	6.7			
63R-7, 80–87	STA	314.6	4.2				
			VeinC	4.1		2.4	
			VeinF	7.0			
65R-3, 54–58	XRF	323.1	5.2				
66R-4, 14–19	STA	329.4	3.4				
67R-3, 74–78	XRF	333.6	4.1				
68R-2, 16–21	XRF	336.7	5.6				
69R-3, 86–92	XRF	344.5	4.3				
69R-3, 86–96	STA	334.5	4.9				
70R-1, 39–49	VAN	346.4	Vein	4.7		2.7	
70R-1, 80–84	XRF	346.8	4.8				
70R-2, 11–13	STA		Vein	5.0		3.3	
				6.6			
71R-2, 129–131	XRF	353.6	6.8				
71R-3, 0–5	XRF	353.9	5.8				
72R-2, 56–62	XRF	358.1	6.0				
72R-7, 42–47	STA	360.1		4.7			
73R-1, 54–57	XRF	366.0	6.0				
74R-6, 115–119	XRF	383.5	5.8				
75R-1, 0–6	STA	385.2	6.0				
75R-5, 27–30	XRF	390.3	6.6				
76R-2, 121–126	STA	396.5	5.5		5.0		4.5
76R-3, 93–97	XRF	397.5	5.7				
77R-2, 4–7	XRF	404.6	6.2				
77R-5, 15–19	STA	409.1	4.7				
78R-1, 132–136	XRF	410.8	6.0				
78R-3, 110–119	STA	413.4	6.6				
			Vein	6.8			
79R-6, 69–77	STA	422.5	6.4	7.5			5.8
79R-6, 90–96	XRF	422.7	5.5				
80R-2, 35–40	XRF	425.8	5.8				
80R-6, 6–9	XRF	431.4	6.4				
80R-7, 27–34	STA	433.1	5.8				
81R-4, 60–68	STA	438.4	6.3		6.5		
81R-5, 1–7	XRF	439.2	6.1				
81R-6, 87–90	STA	441.3		6.9	5.2		
		NAPL	Vein	6.6	5.7		
82R-1, 49–51	XRF	443.5	6.3				
82R-2, 58–65	STA	445.1	7.2		5.6		
82R-7, 21–29	STA	451.8	6.2	6.5			5.6
83R-5, 36–46	STA	460.1	5.1				
83R-7, 77–81	XRF	461.6	5.8				
84R-2, 70–78	STA	464.2	5.7				
84R-5, 80–82	XRF	468.5	5.2				
85R-4, 17–25	STA	476.0	3.0				
85R-7, 79–85	XRF	480.7	4.8				
87R-5, 79–86	STA	497.4	4.9	4.9		5.7	
			Vein		3.8		
87R-7, 7–14	STA		Matrix	3.4			
			VeinC	4.9		1.7	
			VeinF	7.3			
87R-7, 51–55	XRF	499.7	4.6				

Codes are as follows: XRF = whole-rock powder made on shipl VAN = Vanko sample; STA = Stakes sample; KEM = Kempton sample. WR = whole-rock powder. Minerals are PLAG = plagioclase; AMPH = amphibole (usually hornblende; if actinolite then designated with act); DI = diopside; CPX = igneous clinopyroxene; A signifies that mineral is visibly altered; G = gray plagioclase; W = white plagioclase; C = coarse-grained; F = fine-grained.

Petrofabric Studies

A detailed analysis of the deformation has been described by Cannat et al. (this volume), Cannat (this volume), and Dick et al. (b, this volume). Dick et al. (b, this volume) divide the core into five Deformation Zones, based on data collected during a post-cruise redescription of the core. We use the textural classifications developed on board the ship and which were used for the initial core descriptions. Based on the distribution of the deformation intensity, Cannat et al. (this volume) divide the core into three structural domains, which are indicated in Figure 1. The upper structural domain extends from Core 118-735B-1D to 118-735B-35R (0–172 mbsf). This domain is characterized by extensive development of highly deformed types III, IV, and V textures above a 5-m-thick mylonite zone (21–26 mbsf) and a decrease in deformation below. The middle structural domain extends from Core 118-735B-36R to the top of Core 118-735B-56R (172–272 mbsf). In this domain, there is a well-developed magmatic foliation, overprinted by discrete intervals of ductile deformation. The lower structural domain extends from Core 118-735B-77R to the bottom of the hole (403–500 mbsf). Within this lower zone, there is limited development of the most deformed textural types within discrete shear zones. Between the middle and lower structural domains, the gabbros are almost completely free of ductile deformation. (Note that deformation Zones 1 and 2 of Dick et al. [this volume, b] are equivalent to our upper structural domain. Dick et al.'s deformation Zones 3 and 5 are equivalent to our middle and lower structural domains, respectively. Deformation Zone 4 comprises the undeformed interval between our middle and lower structural domains.) Cannat (this volume) identifies four major mylonite zones: one at approximately 21-26 mbsf (Cores 118-735B-5D to 118-735B-6D), one at approximately 35 mbsf (Cores 118-735B-9D to 118-735B-10R), one at 221–224 mbsf (Core 118-735B-46R), and one near the middle of the core at approximately 271 mbsf (Core 118-735B-56R) (see Fig. 1). In addition, there are thin mylonite bands within the lower structural domain that are frequently developed in oxide-rich layers. In the thick mylonite zones, a change in the dip of the foliation from high-angle (10° to 50°) to almost horizontal within a short stratigraphic interval was observed. In addition, the observed shear sense is predominantly extensional within these zones of maximum deformation. These features lead Cannat et al. (this volume) to infer that these mylonite zones are the traces of listric normal faults. These structural domains can be thought of as segments of the core separated by ductile faults that may also delineate major permeability or lithostratigraphic discontinuities within the section. The distribution of metamorphic assemblages, except possibly for the secondary orthopyroxene and olivine, is more closely tied to the structural aspects of the core than to the primary lithology, making this distinction more useful for this discussion.

Brittle Features

Synkinematic

The end of ductile deformation was marked by brittle failure of the rocks. This is characterized by the progressive formation of a synkinematic to post-kinematic network of cracks perpendicular to the foliation: (1) microcracks in porphyroclasts that extend from grain boundary to grain boundary and that are perpendicular to the foliation; (2) continuous cracks resulting from the microcracks interconnecting across bands of neoblasts (grains of secondary plagioclase that grew under metamorphic conditions); and (3) a through-going crack network produced by the opening of the cracks to greater than 0.25-cm wide in some cores. These microcracks are predominantly filled with amphibole (hornblende or edenite) or with amphibole and plagioclase and are most abundant in the upper and middle structural domains.

Post-Kinematic

A second set of fractures is dominant in the lower portion of the core; these are solely post-kinematic or apparently not associated with ductile deformation. Minerals that fill this post-kinematic set of fractures are similar to those observed in the hydrothermal breccias, including diopside, epidote, sodic plagioclase, apatite, sphene, analcime, actinolite, thomsonite, chlorite, and carbonate. Near-vertical hydrothermal veins of diopside and plagioclase crosscut the metamorphic foliation and could be traced through several sections of core. Low-angle thick veins of diopside, sodic plagioclase, sphene, and epidote may include hydrothermally altered felsic intrusions. Undeformed vein assemblages, including early diopside and plagioclase, succeeded by epidote, sphene, chlorite, or zeolites, crosscut deformed and undeformed gabbro intervals between the breccia zones.

In the lower portion of the core (Fig. 1), hydrothermally altered breccia zones are much more abundant than the hornblende vein mineralization that dominated the upper half of the core. The core recovered from the largest brecciated zones was composed of poorly foliated to undeformed gabbro fragments, stained red with Fe-oxide, and crosscut by late veins of carbonate and smectite. Abundant veins weld fragmented pieces together and extend into the adjacent host rock. The host rock for the veins was commonly replaced by assemblages similar to those observed in the vein. We suggest that these brecciated zones are the origin of the vein minerals in fracture systems unrelated to ductile deformation. Cataclastic or breccia zones are systematically associated with the LMIs and probably result from auto-brecciation caused by magmatic hydrofracturing that accompanied the LMI injection. Secondary mineral assemblages within the breccia zones are similar to those found in the LMI, or their hydrothermal replacement, including sodic plagioclase, quartz, mica, diopside, zircon, magnetite, actinolite, epidote, sphene, thomsonite, and analcime and carbonates. The textures of the magmatic/hydrothermal breccia zones vary from extensive static replacement of host rock to replacement of previously brecciated fragments in discrete hydrothermal zones. Zones of brecciation and extensive metamorphic recrystallization were scattered in Cores 118-735B-35R to 118-735B-50R and are common to dominant in Cores 118-735B-56R to 118-735B-76R. Some of these veins suggest contemporaneous shearing. Near the lower portion of the core, there is evidence of crushed hydrothermal assemblages, crosscut by undeformed veins of diopside. This suggests repeated episodes of brecciation, veining, crushing, and veining. Open cracks have been sealed by strongly zoned diopside or hornblende, whose euhedral mineral faces and concentric zoning suggest episodic growth into an open, fluid-filled fracture (Pl. 1, Fig. 3).

METAMORPHIC AND VEIN-FILLING MINERAL ASSEMBLAGES

The secondary mineralogy of Core 118-735B-1D is limited to about a dozen mineral species. This apparent simplicity, however, belies the extraordinary heterogeneity in the distribution of the assemblages and their relationship to late magmatic and crustal deformation processes. There are three main styles of metamorphic recrystallization that can be distinguished in the core:

1. Minerals that are clearly associated with episodes of plastic deformation.
2. Minerals that are associated with the influx of seawater along grain boundaries and open fractures under static conditions.
3. Minerals that are associated with the infiltration of late magmatic intrusions (hydrous LMI). This provoked hydraulic fracturing and cataclasis of the rocks, creating permeable zones subjected to progressively lower grades of metamorphism.

Each style of metamorphic recrystallization actually covers a number of metamorphic assemblages that depend on temperature, availability of water, original rock modal composition, and timing of the penetration of deep faults into a crystallizing magma chamber at high temperatures.

Synkinematic Minerals

Host Rock or Matrix

Rocks that have undergone metamorphic recrystallization under conditions of ductile deformation were found in localized zones throughout the core. Metamorphic minerals include both hydrous and anhydrous phases that have grown subparallel to metamorphic foliation or within pressure shadows of porphyroclasts. The end of this phase of dynamic recrystallization is marked by the synkinematic to late-kinematic veins across porphyroclasts or bands of neoblasts. The zones of deformed rocks are thick near the two fault zones (see Cannat et al., this volume), but narrow shear zones also cut the undeformed gabbros several meters from the faults. Some cores are completely devoid of ductile deformation, whereas a few samples suggest slight degrees of deformation prior to complete magmatic crystallization (Cannat et al., this volume).

Three types of assemblages have been identified as clearly associated with ductile deformation referred to here as the pyroxene-hornblende-plagioclase (PX-HB-PL), hornblende-plagioclase (HB-PL), and actinolitic hornblende-sodic plagioclase (ACT HB-NA PL) assemblages. We suggest that these assemblages represent a progressive decrease in temperature and increase in the activity of H_2O (see "Discussion" section, this chapter). The structural aspects of this deformation are summarized in Cannat et al. (this volume). A summary of pyroxene, amphibole and plagioclase compositions is provided in Tables 2 through 6, with a more extensive compilation of amphibole compositions provided in Vanko and Stakes (this volume).

The earliest formed assemblage is the PX-HB-PL, which is typically granular and nearly anhydrous. This assemblage is made up of polygonal neoblasts crystallizing in the tails of magmatic porphyroclasts and aligned in the foliation plane. It includes plagioclase, clinopyroxene, orthopyroxene, olivine, brown amphibole, and ilmenite depending on the magmatic mineral assemblage. These mineral associations, as well as the granular texture, are typical of granulite facies conditions. Plagioclase neoblasts are compositionally similar to adjacent porphyroclasts within a range of about 5% An content. Neoblasts of clinopyroxene are commonly (although not consistently) slightly more diopsidic than adjacent porphyroclasts. The metamorphic clinopyroxene is distinguished by its pale color and lack of cleavage planes. The cleavage planes of the clinopyroxene porphyroclasts are characteristically coarsened and commonly dotted with blebs of brown hornblende or ilmenite or rarely, dark red rutile. Ilmenite is recrystallized and intergrown with the silicate neoblasts. Some of this ilmenite may have derived from recrystallization of the clinopyroxene porphyroclasts and exclusion of the excess oxide as inferred from ilmenite-filled cracks crossing the clinopyroxene.

Orthopyroxene is sporadically recrystallized into small neoblasts, but more commonly forms crushed crystals around the orthopyroxene porphyroclasts. The rare presence of orthopyroxene neoblasts is diagnostic of temperatures of granulite-grade metamorphism (see later section for calculated temperatures). Oxide-rich mylonite zones commonly have bands of fine-grained ilmenite and magnetite containing small egg-shaped orthopyroxene inclusions; however, it is not certain whether the small grains of orthopyroxene are crushed relicts of igneous phases or neoblasts.

Magmatic red-brown Ti-pargasite is present as a cumulus phase in undeformed gabbros, especially in ferrogabbros, or as blebs within clinopyroxene porphyroclasts. In magmatic amphibole-bearing rocks, a secondary brown parasitic hornblende appears as symplectic intergrowths with clinopyroxene, as well as a well-crystallized synkinematic phase in the bands of foliated minerals in granular assemblages. Postdating the early, mostly anhydrous, granular assemblage, a more hydrous assemblage was characterized by the widespread development of brown to green amphibole. Synkinematic green hornblende joins this assemblage as large, anhedral grains oriented within planes of foliation or in pressure shadows of pyroxene porphroclasts. The green hornblende was not observed as polygonal neoblasts, as was the red-brown hornblende, although large deformed anhedral grains of dark green hornblende are intergrown with brown hornblende in the tails of pyroxene porphyroclasts, suggesting that these two phases were contemporaneous.

The boundary between the high-grade PX-HB-PL and medium-grade HB-PL recrystallization was arbitrarily chosen as the disappearance of recrystallized clinopyroxene. At this point in the metamorphic history, light brown to green coarse amphibole, rather than pyroxene, was stabilized. This medium-grade dynamic metamorphic assemblage includes plagioclase, oxide (mostly ilmenite), and an abundance of green and brown amphibole, with brown mica in a few samples. Plagioclase neoblasts associated with this stage of metamorphism tend to be small and poorly polygonized. Abundant green and brown hornblende was observed as neoblasts replacing clinopyroxene, intergrown with plagioclase in the foliation, and intergrown with oxide in the tails of clinopyroxene porphyroclasts.

The assemblage that marks the terminal stage of hydrous ductile deformation is the ACT HB-NA-PL assemblage composed of actinolitic hornblende and plagioclase of intermediate to sodic composition. At this stage of metamorphism, most porphyroclasts have recrystallized to secondary minerals. This stage of ductile deformation was characteristically localized, and often only affected a few foliation planes within a thin section. Plagioclase neoblasts are small and intergrown with pale green to yellow acicular amphibole. The composition of the phases in this assemblage overlaps the composition of phases associated with the pseudomorphous and coronitic replacements under static conditions. This suggests that at this stage in the metamorphic history, limited portions of the core underwent ductile deformation, while other portions cracked under brittle conditions, leading to enhanced penetration by seawater.

Veins

Detailed phase chemistry, fluid inclusions, and oxygen isotope compositions of vein minerals have been provided in Vanko and Stakes (this volume). Here, we provide an overview of the mineralogy of the vein assemblages within the context of the

Table 2. Pyroxene prophyroclasts and neoblasts from deformed gabbros and magmatic pyroxenes from the late magmatic intrusives (LMI).

Analysis:	1	2	3	4	5	6	7	8	9	10	11	12	13	14	15	16	17	18	19	20	21	22	23
SiO_2	52.35	51.59	52.14	54.15	51.95	52.58	52.27	51.92	51.85	50.96	51.00	51.79	50.82	50.64	51.58	51.98	51.99	51.92	52.10	52.22	51.36	51.85	51.59
TiO_2	0.68	0.60	0.84	0.54	0.45	0.41	0.51	0.50	0.14	0.38	0.14	0.00	0.46	0.48	0.13	0.15	0.75	0.19	0.39	0.16	0.44	0.14	0.88
Al_2O_3	2.97	3.48	2.95	2.42	1.34	1.45	1.79	2.40	0.65	1.21	0.62	0.17	1.67	1.21	0.75	0.75	2.76	1.12	1.56	0.59	1.67	0.65	2.43
Fe_2O_3	0.00	0.00	0.00	0.00	0.73	0.00	0.00	0.99	0.00	0.69	1.12	0.19	0.09	2.74	1.99	1.46	1.07	0.62	0.58	0.50	1.53	0.00	0.99
FeO	5.74	6.41	5.78	5.61	11.06	10.83	10.71	6.47	11.93	13.56	10.53	12.38	13.62	15.31	11.06	11.64	7.36	11.22	10.65	12.05	10.48	11.93	10.04
MnO	0.20	0.17	0.22	0.18	0.42	0.37	0.48	0.24	0.49	0.47	0.43	0.49	0.52	0.55	0.52	0.41	0.19	0.45	0.37	0.38	0.47	0.49	0.27
MgO	15.52	15.88	15.40	16.80	13.83	13.21	13.20	14.61	11.96	12.68	12.07	10.57	12.39	11.64	12.24	12.05	15.69	13.03	13.01	12.53	12.63	11.96	14.84
CaO	21.72	20.22	22.39	20.28	19.22	20.70	20.39	21.70	20.92	18.02	21.57	22.41	18.13	17.11	20.64	20.96	19.43	20.12	20.52	20.38	20.59	20.92	18.38
Na_2O	0.36	0.70	0.39	0.38	0.40	0.38	0.40	0.44	0.29	0.34	0.21	0.19	0.37	0.53	0.42	0.41	0.52	0.34	0.46	0.37	0.43	0.29	0.47
Cr_2O_3	0.09	0.12	0.07	0.06	0.02	0.02	0.10	0.22	0.00	0.00	0.00	0.03	0.00	0.00	0.00	0.00	0.08	0.02	0.02	0.02	0.03	0.00	0.00
Sum	99.63	99.37	100.27	100.42	99.31	99.79	99.54	99.46	98.23	98.28	97.70	98.22	98.07	100.21	99.33	99.81	99.80	99.02	99.68	99.21	99.63	98.23	99.89
Si	1.929	1.903	1.913	1.964	1.962	1.974	1.965	1.932	1.994	1.964	1.974	2.007	1.961	1.939	1.967	1.973	1.922	1.973	1.989	1.988	1.943	1.994	1.925
Ti	0.019	0.017	0.023	0.015	0.013	0.012	0.015	0.014	0.004	0.011	0.004	0.000	0.013	0.014	0.003	0.004	0.021	0.005	0.003	0.005	0.013	0.004	0.025
Al	0.129	0.151	0.128	0.103	0.060	0.064	0.079	0.105	0.030	0.055	0.028	0.008	0.076	0.055	0.034	0.033	0.119	0.050	0.028	0.026	0.074	0.030	0.107
Fe^{3+}	0.000	0.056	0.026	0.000	0.021	0.000	0.000	0.028	0.000	0.020	0.032	0.005	0.003	0.079	0.057	0.043	0.030	0.018	0.016	0.014	0.044	0.000	0.028
Fe^{2+}	0.177	0.142	0.152	0.170	0.349	0.340	0.337	0.201	0.384	0.437	0.341	0.401	0.440	0.490	0.352	0.370	0.228	0.357	0.383	0.384	0.332	0.384	0.313
Mn	0.006	0.005	0.007	0.006	0.010	0.007	0.005	0.006	0.016	0.015	0.014	0.016	0.017	0.018	0.016	0.013	0.006	0.014	0.014	0.012	0.015	0.016	0.009
Mg	0.852	0.873	0.842	0.908	0.778	0.739	0.740	0.810	0.686	0.728	0.696	0.611	0.712	0.664	0.696	0.682	0.865	0.738	0.714	0.711	0.712	0.686	0.825
Ca	0.858	0.799	0.880	0.788	0.778	0.833	0.821	0.865	0.862	0.744	0.895	0.931	0.750	0.702	0.843	0.852	0.770	0.819	0.825	0.831	0.835	0.862	0.735
Na	0.026	0.050	0.028	0.027	0.029	0.028	0.029	0.031	0.021	0.025	0.016	0.014	0.028	0.039	0.031	0.030	0.038	0.025	0.028	0.027	0.031	0.021	0.034
Cr	0.003	0.003	0.002	0.002	0.001	0.001	0.003	0.006	0.000	0.000	0.000	0.001	0.000	0.000	0.000	0.000	0.002	0.001	0.000	0.001	0.001	0.000	0.000
Catsum	3.999	4.000	4.000	3.982	4.000	3.996	3.994	4.000	3.997	4.000	4.000	3.993	4.000	4.000	4.000	4.000	4.000	4.000	4.000	4.000	4.000	3.997	4.000
Wo	45.4	44.7	46.9	42.2	40.8	43.6	43.3	46.1	44.6	39.0	46.3	47.9	39.4	37.4	44.2	44.5	41.3	42.8	42.9	43.2	44.4	44.6	39.2
En	45.2	48.1	44.9	48.7	40.9	38.6	39.0	43.2	35.5	38.1	36.0	31.4	37.5	35.4	36.5	35.6	46.4	38.6	37.1	36.9	37.9	35.5	44.1
Fs	9.4	7.8	8.1	9.1	18.3	17.8	17.7	10.7	19.9	22.9	17.6	20.7	23.1	27.1	19.3	20.0	12.2	18.6	19.9	19.9	17.7	19.9	16.7

Pyroxene formulas were calculated using the formulas of Papike et al. (1974) and a program provided by P. Meyer. Analyses are from the following samples: Sample 118-735B-19R-2, 98–100 cm, Pc. 12 (1–4); Sample 118-735B-37R-2, 113–117 cm, Pc. 1H (5–8); Sample 118-735B-53R-4, 5–15 cm, Pc. 1B (9–13); Sample 118-735B-56R-2, 18–22 cm, Pc. 2B (14–16); Sample 118-735B-58R-2, 10–17 cm, Pc. 1B (17); Sample 118-735-73R-6, 8–10 cm, Pc. 1B (18–22); Sample 118-735B-5R-2, 11–18 cm, Pc. 1B (23). Relict prophyroclasts in deformed gabbros included analyses 1, 4, 5, 7, 8, 10, 13, 14–15 (core and rim, respectively, of one grain). Recrystallized pyroxene and neoblasts include analyses 2, 3, 5, 6, 9, 11, 16 Analysis 12 is from a vein of LMI, and Analyses 18–22 are a range of compositions from a zone impregnated by LMI. Analyses 17 and 23 are relict igneous augite.

Table 3. **Pyroxene compositions from breccias and veins.**

Analysis:	1	2	3	4	5	6	7	8	9	10	11	12	13	14	15	16	17	18	19	20	21	22	23
SiO_2	52.13	52.30	50.48	51.79	52.28	51.36	51.27	54.19	53.92	51.11	53.73	54.65	52.97	50.90	51.34	54.02	52.82	53.00	53.59	53.08	52.75	53.06	53.87
TiO_2	0.06	0.04	0.62	0.69	0.34	0.42	0.43	0.02	0.00	0.01	0.00	0.01	0.29	0.75	0.83	0.04	0.04	0.03	0.19	0.00	0.05	0.05	0.09
Al_2O_3	0.22	0.25	2.91	2.79	1.64	1.86	1.75	0.27	0.24	0.72	0.06	0.36	1.35	2.93	2.60	0.46	0.38	0.47	1.63	0.26	0.69	0.65	1.08
Fe_2O_3	0.92	1.01	4.39	2.96	2.69	3.59	2.72	1.16	1.09	1.49	0.40	0.89	2.34	5.06	3.89	0.47	1.11	0.00	0.00	1.72	1.76	2.31	1.45
FeO	8.72	8.96	4.18	5.95	5.14	4.90	5.28	3.22	3.70	9.54	6.94	0.73	3.38	1.57	2.52	5.23	5.91	5.99	5.10	6.16	5.21	5.40	3.93
MnO	0.28	0.37	0.21	0.31	0.26	0.26	0.32	0.09	0.07	0.36	0.04	0.03	0.23	0.21	0.16	0.07	0.11	0.23	0.09	0.00	0.00	0.00	0.00
MgO	13.43	13.23	14.93	15.88	15.38	14.83	15.18	16.19	15.94	11.47	14.03	17.53	16.14	16.09	15.77	15.08	14.41	14.19	15.12	14.01	15.51	13.99	15.09
CaO	24.27	23.77	21.84	20.46	22.62	22.34	22.34	25.34	25.51	25.15	25.68	26.40	23.53	21.45	22.57	24.37	24.42	24.08	3.28	24.56	22.95	24.70	25.30
Na_2O	0.27	0.27	0.42	0.39	0.32	0.31	0.35	0.30	0.28	0.14	0.12	0.140	0.38	0.86	0.67	0.27	0.24	0.09	0.39	0.51	0.32	0.54	0.27
Cr_2O_3	0.00	0.01	0.01	0.00	0.01	0.03	0.04	0.00	0.00	0.00	0.00	0.00	0.17	0.23	0.25	0.00	0.00	0.00	0.12	0.00	0.03	0.00	0.00
Sum	100.30	100.21	99.99	101.22	100.67	99.53	99.68	100.76	100.75	99.98	101.00	100.74	100.78	100.05	100.59	100.01	99.43	98.09	99.50	100.29	99.26	100.70	101.08
Si	1.960	1.967	1.873	1.894	1.924	1.916	1.911	1.976	1.973	1.945	1.985	1.974	1.935	1.869	1.881	1.992	1.974	1.998	1.977	1.973	1.964	1.961	1.964
Ti	0.002	0.001	0.017	0.019	0.009	0.001	0.012	0.000	0.000	0.000	0.000	0.000	0.008	0.021	0.023	0.001	0.001	0.001	0.005	0.000	0.001	0.001	0.002
Al	0.010	0.011	0.127	0.121	0.071	0.082	0.077	0.011	0.010	0.032	0.003	0.015	0.058	0.127	0.112	0.020	0.017	0.021	0.071	0.011	0.030	0.028	0.046
Fe^{3+}	0.026	0.029	0.122	0.081	0.074	0.101	0.076	0.032	0.030	0.043	0.011	0.025	0.064	0.140	0.107	0.013	0.031	0.000	0.000	0.048	0.049	0.064	0.040
Fe^{2+}	0.274	0.282	0.130	0.182	0.158	0.153	0.165	0.098	0.113	0.304	0.214	0.022	0.103	0.048	0.077	0.161	0.185	0.189	0.157	0.191	0.162	0.167	0.120
Mn	0.009	0.012	0.007	0.009	0.008	0.008	0.010	0.003	0.002	0.012	0.001	0.001	0.007	0.006	0.005	0.002	0.003	0.007	0.003	0.000	0.000	0.000	0.000
Mg	0.753	0.742	0.826	0.865	0.844	0.824	0.843	0.880	0.869	0.650	0.773	0.943	0.878	0.881	0.861	0.828	0.803	0.797	0.831	0.776	0.861	0.771	0.820
Ca	0.978	0.958	0.868	0.801	0.892	0.893	0.892	0.990	1.000	1.026	1.017	1.021	0.921	0.844	0.886	0.963	0.978	0.973	0.920	0.978	0.915	0.978	0.989
Na	0.020	0.020	0.030	0.027	0.023	0.022	0.025	0.021	0.020	0.011	0.008	0.010	0.027	0.061	0.048	0.019	0.017	0.007	0.028	0.037	0.023	0.039	0.019
Cr	0.000	0.000	0.000	0.000	0.000	0.001	0.001	0.000	0.000	0.000	0.000	0.000	0.005	0.007	0.007	0.000	0.000	0.000	0.003	0.000	0.001	0.000	0.000
Catsum	4.031	4.022	4.000	4.000	4.005	4.002	4.012	4.012	4.017	4.022	4.012	4.011	4.007	4.004	4.007	4.000	4.009	3.994	3.995	4.015	4.006	4.010	4.000
Wo	48.8	48.3	47.6	43.4	47.1	47.8	46.9	50.3	50.5	51.8	50.7	51.4	48.4	47.7	48.6	49.3	49.8	49.7	48.2	50.3	47.2	51.1	51.3
En	37.5	37.4	45.3	46.8	44.5	44.1	44.4	44.7	43.8	32.9	38.6	47.5	46.2	49.7	47.2	42.4	40.8	40.7	43.6	39.9	44.4	40.3	42.5
Fs	13.7	14.2	7.1	9.8	8.4	8.2	8.7	5.0	5.7	15.3	10.7	1.1	5.4	2.7	4.3	8.3	9.4	9.7	8.2	9.9	8.4	8.7	6.2

All compositions corrected after Papike et al. (1974) from a program provided by P. Meyer. Data are from the following samples: Sample 118-735B-45R-4, 136–140 cm, Pc. 7 (1–7); Sample 118-735B-64R-4, 73–76 cm, Pc. 1H (8–15); Sample 118-735B-66R-4, 14–19 cm, Pc. 4 (16–19); Sample 118-735B-70R-2, 8–10 cm, Pc. 2 (20–23).

Table 4. Pyroxene compositions for temperature calculations of granulite grade metamorphism associated with ductile deformation.

Analysis:	1	2	3	4	5	6	7	8
SiO_2	51.99	52.11	52.39	52.13	55.76	55.61	54.07	53.82
TiO_2	0.12	0.08	0.21	0.33	0.02	0.01	0.10	0.08
Al_2O_3	0.36	0.46	1.04	1.29	0.37	0.32	0.46	0.49
Fe_2O_3	0.14	0.33	1.03	0.65	0.00	0.00	0.00	0.00
FeO	25.38	25.02	9.32	10.45	13.83	14.37	5.83	5.75
MnO	0.78	0.88	0.40	0.37	0.28	0.36	0.18	0.22
MgO	19.64	20.15	13.50	13.08	29.14	28.56	15.36	15.43
CaO	0.83	0.40	21.41	20.94	0.32	0.34	23.10	23.06
Na_2O	0.01	0.01	0.35	0.36	0.01	0.01	0.20	0.20
Cr_2O_3	0.00	0.01	0.03	0.03	0.00	0.02	0.10	0.10
Sum	99.24	99.44	99.67	99.63	99.73	99.60	99.40	99.15
Si	1.987	1.983	1.969	1.966	1.994	1.997	2.002	1.998
Ti	0.003	0.002	0.006	0.009	0.001	0.000	0.003	0.002
Al	0.016	0.021	0.046	0.057	0.016	0.014	0.020	0.021
Fe^{3+}	0.004	0.009	0.029	0.018	0.000	0.000	0.000	0.000
Fe^{2+}	0.811	0.796	0.293	0.329	0.414	0.432	0.180	0.179
Mn	0.025	0.028	0.013	0.012	0.008	0.011	0.006	0.007
Mg	1.119	1.143	0.756	0.735	1.553	1.528	0.847	0.854
Ca	0.034	0.016	0.862	0.846	0.012	0.013	0.916	0.917
Na	0.001	0.001	0.026	0.026	0.001	0.001	0.014	0.014
Cr	0.000	0.000	0.001	0.001	0.000	0.001	0.003	0.003
Catsum	4.000	4.000	4.000	4.000	3.998	3.996	3.991	3.995
Wo	1.7	0.8	45.1	44.3	0.6	0.7	47.1	47.0
En	56.9	58.4	39.5	38.4	78.4	77.4	43.6	43.8
Fs	41.3	40.7	15.3	17.2	20.9	21.8	9.2	9.1

NOTE: Formulas are calculated after Papike et al. (1974) using a program provided by P. Meyer. Analyses pairs are recrystallized grains that were in contact, apparently in equilibrium. Analyses 1 through 4 are from Sample 118-735B-8D-1, Pc. 4. Analyses 5 through 8 are from Sample 118-735B-46R-3, Pc. 2B. Equilibrium temperatures calculated using Wells (1977) are as follows: For analyses pair 1 and 3, T = 894°C; for analyses pair 2 and 4, T = 908°C; for analyses pair 5 and 7, T = 852°C; for analyses pair 6 and 8, T = 849°C.

metamorphic history. Hornblende dominates as a vein mineral in the upper structural unit of the core, joined by plagioclase in the middle structural unit. Hornblende compositions vary from brilliant green, strongly zoned ferroan pargasite to edenitic or actinolitic hornblende, illustrated in Figure 2. The vein hornblendes compositionally overlap the synkinematic green hornblende as well as the hornblende that fills the extensional microcracks, suggesting that they form contemporaneously, under similar conditions. In deformed zones that are cut by the wider veins, the vein hornblende smoothly grades into adjacent foliation planes, with no obvious optical or compositional break from vein to foliation-plane mineral phase.

Post-Kinematic Minerals

Pseudomorphs and Coronas

Hydrous alteration under static conditions apparently is spatially related to the presence of synkinematic cracks or veins. These minerals are predominantly hydrous and characteristically replace the deformation-episode minerals, both along planes of foliation and adjacent to the synkinematic vein network (Pl. 1, Fig. 4). Even the smallest partially healed cracks are delineated by minute, but observable quantities of secondary minerals. The result of this static metamorphic recrystallization is characteristically zoned pseudomorphous or coronitic replacements that are dependent on the primary modal composition of the rocks. Except for a few discrete zones in the lower half of the core (e.g., portions of Cores 118-735B-59R to 118-735B-62R; 118-735B-65R; 118-735B-68R to 118-735B-69R; 118-735B-72R; 118-735B-75R to 118-735B-76R 118-735B-79R to 118-735B-80R; 118-735B-82R have less than 5% replacement), there is pervasive hydrous alteration. In zones having only trace amounts of hydrous replacement, olivine or orthopyroxene has been replaced by talc, plagioclase has been replaced by sodic plagioclase and/or magnesio-hornblende, and clinopyroxene has been replaced by actinolite or hornblende. With increasing quantity of hydrous alteration, more complex pseudomorphous replacements develop, including chlorite, pargasite, and mica developing at olivine-plagioclase grain boundaries and tremolite, anthophyllite, or cummingtonite replacing olivine. A column for the presence of amphibole in Figure 1 thus would be a practically solid line representing several types of replacements.

Cores of orthopyroxene or olivine crystals were replaced by intergrowths of talc-tremolite and secondary magnetite. Often surrounding these cores is a zone of Fe-Mg amphibole–anthophyllite or cummingtonite. Along plagioclase-olivine grain boundaries, a zone of pargasite intergrown with phlogopite was frequently observed. The margin of plagioclase often has an outer fringe of actinolite with cuspate zones of pale chlorite that project into the mineral (Pl. 1, Fig. 5). The plagioclase has been sparsely replaced by clinozoisite. Clinopyroxene porphyroclasts and bands of neoblasts frequently have been replaced by green to yellow fibrous amphibole (actinolite to actinolitic hornblende) and plagioclase neoblasts in mosaic bands were replaced by actinolite. Ilmenite was replaced by sphene.

In regions of low-temperature oxidation, orthopyroxene or olivine pseudomorphs have been replaced with cores of carbonate with iddingsite (smectite plus Fe-oxide). Chlorite has been stained red or replaced by Fe-stained smectite. This oxidative alteration was most common in the upper 50 m of the core or adjacent to the larger brecciated zones (Table 7).

Alteration Near Late Intrusives

The stratigraphic relationship between the leucocratic veins and the appearance of zircon argues strongly for the presence of magmatic fluids, in at least the early stages of

Table 5. Representative plagioclase compositions from metagabbroic rocks and late magmatic intrusives.

Analysis:	1	2	3	4	5	6	7	8	9	10	11	12	13	14	15	16
SiO_2	54.08	54.71	54.30	60.27	55.03	67.18	59.93	63.27	54.45	61.23	72.32	53.08	58.60	63.09	57.88	62.23
TiO_2	0.01	0.05	0.08	0.00	0.00	0.00	N.D.	N.D.								
Al_2O_3	29.76	30.09	29.56	25.92	29.38	21.95	25.61	23.26	29.68	25.32	19.96	30.79	26.93	23.25	27.33	24.31
FeO*	0.07	0.06	0.14	0.12	0.01	0.18	0.06	0.10	0.17	0.03	0.12	0.17	0.11	0.08	0.09	0.15
MnO	0.00	0.00	0.00	0.01	0.01	0.00	N.D.	N.D.								
MgO	0.00	0.00	0.02	0.01	0.00	0.00	0.00	0.00	0.00	0.01	0.00	0.00	0.00	0.00	0.01	0.01
CaO	11.76	12.06	11.59	7.24	11.67	2.68	6.25	3.54	11.14	5.53	0.09	12.03	6.63	3.73	8.15	4.74
Na_2O	4.46	4.25	4.59	6.98	4.60	8.15	7.30	8.79	4.87	7.77	9.52	4.23	7.01	8.66	6.19	8.04
K_2O	0.00	0.02	0.00	0.04	0.01	0.04	0.09	0.06	0.01	0.01	0.02	0.00	0.01	0.03	0.24	0.27
Sum	100.15	101.24	100.29	100.59	100.86	100.17	99.24	99.04	100.34	99.92	102.04	100.29	99.29	98.86	99.90	99.75
Si	2.433	2.434	2.441	2.663	2.458	2.919	2.684	2.810	2.444	2.710	3.055	2.389	2.621	2.807	2.586	2.756
Ti	0.000	0.002	0.003	0.000	0.000	0.000										
Al	1.578	1.578	1.566	1.350	1.546	1.124	1.338	1.217	1.570	1.321	0.994	1.633	1.420	1.219	1.439	1.268
Fe	0.003	0.003	0.005	0.004	0.005	0.006	0.003	0.004	0.006	0.001	0.004	0.006	0.004	0.003	0.003	0.005
Mn	0.000	0.000	0.000	0.013	0.013	0.000										
Mg	0.000	0.000	0.001	0.001	0.000	0.000	0.000	0.000	0.000	0.001	0.000	0.000	0.000	0.000	0.001	0.001
Ca	0.567	0.575	0.558	0.343	0.558	0.125	0.296	0.169	0.536	0.262	0.004	0.580	0.318	0.178	0.390	0.225
Na	0.389	0.366	0.400	0.598	0.399	0.687	0.642	0.757	0.424	0.667	0.780	0.369	0.608	0.748	0.536	0.690
K	0.000	0.001	0.000	0.041	0.008	0.002	0.007	0.003	0.001	0.001	0.001	0.000	0.001	0.002	0.014	0.015
Catsum	4.971	4.958	4.974	4.962	4.968	4.863	4.970	4.960	4.980	4.963	4.837	4.976	4.971	4.956	4.968	4.960
AB	40.7	38.9	41.8	63.42	41.6	84.4	68.0	81.5	44.1	71.7	99.3	38.5	65.6	80.6	57.0	74.2
OR	0.0	0.1	0.0	0.2	0.1	0.3	0.7	0.4	0.0	0.1	0.2	0.0	0.1	0.2	1.5	1.6
AN	59.3	61.0	58.2	36.3	58.3	15.3	31.3	18.13	55.8	28.2	0.5	61.5	34.3	19.2	41.5	24.2

Note: All formulas calculated on the basis of eight oxygens. N.D. = not determined. Analyses 1 through 3 are from Sample 118-735B-19R-2, Pc. 12 (98–100 cm). Analysis 1 is a neoblast intergrown with endenitic hornblende. Analysis 2 is typical relict igneous porphyoclast. Analysis 3 is a heavily veined relict igenous crystal. Analyses 4 through 6 are from Sample 118-735B-37R-2, Pc. 1H (113–117 cm). Analysis 4 is a neoblast; Analysis 5 is the edge of a relict-veined porphyroclast; and Analysis 6 is metamorphic plagioclase intergrown with epidote and actinolite. Analyses 7 and 8 are from Sample 118-735B-53R-4, Pc. 1B ((5–15 cm), a foliated metagabbro cut by a LMI vein. Analysis 7 is a porphyroclast from the host metagabbro, and Analysis 8 is a grain from the LMI vein, adjacent to a grain of zircon. Analyses 9 through 11 are from Sample 118-735B-58R-2, Pc. 1B (10–17 cm). Analysis 9 is an inclusion of igneous plagioclase in clinopyroxene, Analysis 10 is a neoblast, and Analysis 11 is altered pagioclase within a mylonite zone. Analyses 12 through 14 are from Sample 118-735B-66R-4, Pc. 4 (14–19 cm), a metagabbro cut by shears and heavily veined by diopside and plagioclase. Analysis 12 is the core of a large grain in a sheared region, and Analysis 13 is the crushed edge of the same grain. Analysis 14 is sodic plagioclase in the shear, with a diopside vein. Analyses 15 and 16 are from Sample 118-735B-73R-6, Pc. 1B (8–10 cm). Analysis 15 is the center of a relict igenous plagioclase, while Analysis 16 is a small euhedral grain from the center of an invading LMI vein.

Table 6. Representative amphibole compositions from metagabbros and late magmatic intrusives from Hole 735B.

Analysis:	1	2	3	4	5	6	7	8	9	10	11	12	13	14	15	16
SiO_2	44.19	45.65	44.02	49.51	50.37	38.69	38.84	51.54	57.75	52.29	48.30	43.27	43.58	43.42	51.74	53.31
TiO_2	3.41	0.78	3.85	0.57	0.74	0.00	0.20	0.042	0.04	0.55	1.23	3.38	2.98	3.63	0.13	0.17
Al_2O_3	11.32	9.07	11.29	5.21	3.97	17.46	14.37	4.23	0.77	4.36	4.92	11.51	11.44	11.60	2.87	1.30
FeO*	8.71	14.20	9.06	13.63	16.95	15.56	22.33	13.32	4.70	9.91	16.48	13.17	10.73	12.20	21.64	21.77
MnO	0.11	0.16	0.14	0.15	0.30	0.26	0.28	0.13	0.14	0.07	0.27	0.24	0.20	0.17	0.29	0.69
MgO	15.23	13.35	14.50	14.47	14.09	10.39	7.22	15.29	22.66	16.56	12.83	12.11	13.90	12.68	11.23	17.48
CaO	11.75	11.98	11.93	12.01	10.77	11.66	11.85	11.89	11.99	12.38	10.25	10.80	11.21	11.07	10.77	3.78
Na_2O	2.59	1.58	2.04	1.20	1.04	3.16	2.77	0.87	0.25	0.70	1.57	2.88	2.84	2.72	0.56	0.29
K_2O	0.02	0.19	0.03	0.07	0.15	0.30	0.35	0.04	0.00	0.04	0.28	0.30	0.24	0.27	0.40	0.01
Cl	0.01	0.23	0.00	0.07	0.01	0.18	0.51	0.05	0.00	0.00	0.00	0.00	0.00	0.00	0.00	0.00
Sum	97.33	97.20	96.86	96.89	98.38	97.66	98.71	97.78	98.30	96.86	96.13	97.56	97.12	97.76	99.62	98.76
-O=Cl,F	0.00	0.05	0.00	0.02	0.00	0.04	0.11	0.01	0.00	0.00	0.00	0.00	0.00	0.00	0.00	0.00
Sum	97.33	97.15	96.86	96.87	98.38	97.62	98.60	97.77	98.30	96.86	96.13	97.56	97.12	97.76	99.62	98.76
Si	6.371	6.680	6.391	7.218	7.366	5.716	5.898	7.372	7.914	7.480	7.262	6.350	6.353	6.337	7.621	7.744
Al	1.629	1.320	1.609	0.782	0.634	2.284	2.102	0.628	0.086	0.520	0.738	1.650	1.647	1.663	0.379	0.256
Sum in T	8.000	8.000	8.000	8.000	8.000	8.000	8.000	8.000	8.000	8.000	8.000	8.000	8.000	8.000	8.000	8.000
Al	0.296	0.246	0.324	0.114	0.051	0.729	0.471	0.086	0.039	0.216	0.135	0.343	0.320	0.334	0.119	0.033
Fe^{3+}	0.234	0.661	0.153	0.440	0.098	0.872	0.844	0.558	0.000	0.188	−0.001	0.310	0.323	0.251	−0.002	0.000
Ti	0.369	0.086	0.420	0.062	0.081	0.000	0.023	0.045	0.004	0.059	0.139	0.362	0.327	0.398	0.014	0.019
Mg	3.272	2.911	3.138	3.144	3.071	2.287	1.633	3.260	4.528	3.531	2.875	2.649	3.020	2.758	2.464	3.785
Fe^{2+}	0.815	1.077	0.947	1.221	1.699	1.050	1.993	1.036	0.329	0.997	1.852	1.306	0.985	1.238	2.405	1.230
Mn	0.013	0.020	0.018	0.019	0.000	0.032	0.037	0.016	0.000	0.008	0.000	0.030	0.025	0.021	0.000	0.000
Ca	0.000	0.000	0.000	0.000	0.000	0.000	0.000	0.000	0.000	0.000	0.000	0.000	0.000	0.000	0.000	0.000
Sum in C	5.000	5.000	5.000	5.000	5.000	5.000	5.000	5.000	5.000	5.000	5.000	5.000	5.000	5.000	5.000	5.000
Fe^{2+}	0.000	0.000	0.000	0.276	0.000	0.000	0.000	0.209	0.000	0.221	0.000	0.000	0.000	0.125	1.415	0.000
Mn	0.000	0.000	0.000	0.000	0.037	0.000	0.000	0.000	0.016	0.000	0.034	0.000	0.000	0.000	0.036	0.080
Ca	1.816	1.879	1.856	1.876	1.688	1.846	1.929	1.822	1.761	1.898	1.651	1.698	1.751	1.731	1.682	0.505
Na	0.184	0.121	0.144	0.124	0.000	0.154	0.071	0.178	0.014	0.102	0.093	0.302	0.249	0.269	0.157	0.000
Sum in B	2.000	2.000	2.000	2.000	2.000	2.000	2.000	2.000	2.000	2.000	2.000	2.000	2.000	2.000	2.000	2.000
Ca	0.000	0.000	0.000	0.000	0.000	0.000	0.000	0.000	0.000	0.000	0.000	0.000	0.000	0.000	0.000	0.084
Na	0.540	0.328	0.429	0.214	0.294	0.750	0.746	0.064	0.053	0.092	0.365	0.518	0.554	0.501	0.000	0.083
K	0.004	0.035	0.006	0.012	0.028	0.057	0.067	0.007	0.000	0.007	0.054	0.056	0.045	0.050	0.074	0.001
Sum in A	0.544	0.363	0.435	0.227	0.322	0.807	0.813	0.071	0.053	0.099	0.419	0.574	0.599	0.551	0.074	0.168
Cl	0.002	0.057	0.000	0.018	0.033	0.044	0.130	0.012	0.000	0.000	0.000	0.000	0.000	0.000	0.074	0.000

NOTE: Amphibole formulas were calculated after Robinson et al. (1982). See Vanko and Stakes (this volume) for a complete explanation of procedure. Most formulas are based on 13 atoms, except Ca, Na, and K (=13ECNK), although a few are based on all Fe as ferrous iron (=FE^{2+}), or 15 atoms, except Na and K (=15ENK). Analyses 1 through 4 are from Sample 118-735B-19R-2D, Pc. 12c (98–100 cm) and all are 13ECNK recalculations. Analyses 1 is brown blebs of magmatic pargasitic hornblende in clinopyroxene. Analyses 2 is green magnesio-hornblende within a synkinematic crack. Analyses 3 and 4 are intergrown neoblasts of brown tschermakitic and green magnesio-hornblende, respectively. Analyses 5 is an actinolitic hornblende (15ENK), replacing clinopyroxene from Sample 118-735B35R-2, Pc. 4G (105–108 cm). Analyses 6 and 7 are both from Sample 118-735B-35R-7, Pc. 2 (14–17 cm), and both are magnesian hastingsites, based on 13ECNK recalculations. Analysis 6 is a dark brown-to-green phase intergrown with phlogopite and forming a corona between olivine and plagioclase. The stoichiometry is also consistent with a calcium mica, but this was not confirmed by the optical properties. Analysis 7 is a large, green, chlorine-bearing phase in a synkinematic vein. Analyses 8 and 9 are from Sample 118-735B-58R-2, Pc. 1B (10–17 cm). Analysis 8 is a synkinematic actinolitic hornblende (based on 13ECNK) found in the tail of a pyroxene augen in a thin mylonite zone. Analysis 9 is a tremolite (FE^{2+}) found as a coronitic replacement of olivine. Analysis 10 is a fringe of actinolitic hornblende (13ECNK) found on a grain of diopside in Sample 118-735B66R-4, Pc. 4, (14–19 cm). Analysis 11 is from an LMI vein in Sample 118-735B73R-6, Pc. 1B (8–10 cm). This brown actinolitic hornblende (FE^{2+}) was surrounded by sodic plagioclase (An_{25}). Analyses 12 through 14 are from Sample 118-735B-85R-4, Pc. 1C (17–25 cm) and were all recalculated as 13ECNK. Analysis 12 is a brown, synkinematic, ferroan pargasitic hornblende. Analysis 13 is a large euhedral paragasitic hornblende in a synkinematic vein. Analysis 14 is a dark, bladed, ferroan, paragasitic hornblende replacing clinopyroxene. Analysis 15 is an iron-rich actinolite (15ENK) that replaces plagioclase in Sample 118-735B-87R-5, Pc. 3 (20–22 cm). Analysis 16 is a cummingtonite that forms a brown rim on clinopyroxene in the same sample.

formation. We suggest that the diopside, zircon, sodic plagioclase, apatite, quartz, and brown amphibole may have crystallized from either an evolved hydrous magma or from a hydrothermal fluid, some of which may be derived from a magmatic source (i.e., a deuteric fluid). The distinction is not always obvious. The magmatic injections may be surrounded by metamorphic aureoles composed of metagabbro gabbro cut by hydrothermal veins that contain similar mineral phases. The magmatic intrusions may themselves be hydrothermally altered. Epidote, sphene, and chlorite obviously formed from a hydrothermal fluid, but are frequently associated with the LMI as lower temperature replacement phases.

Magmatic/Hydrothermal Breccias

Clearly, some of the breccia zones are spatially related to injection of late magmatic liquids, whereas other zones are clearly metamorphic in origin, although they share many of the same phases. The brecciation produced permeable zones that may have allowed cold seawater to penetrate in discrete parts of the lower crust to form progressively lower temperature mineral assemblages, before being sealed by late precipitation of carbonate or smectite. These breccia zones typically define regions of lower temperature metamorphic mineralization (from greenschist to below zeolite grade). These horizons are the only portions of the core in which abundant greenschist grade minerals were found, including green epidote (compared to the paler clinozoisite of the upper core), chlorite, and actinolite (Liou et al., 1974). Epidote appears in these horizons as a vein mineral as well as a replacement of plagioclase. The Fe-poor composition of the epidote suggests temperatures of upper greenschist facies (300°–400°C; Maruyama et al., 1983). Plagioclase is cut by anastomosing veins of

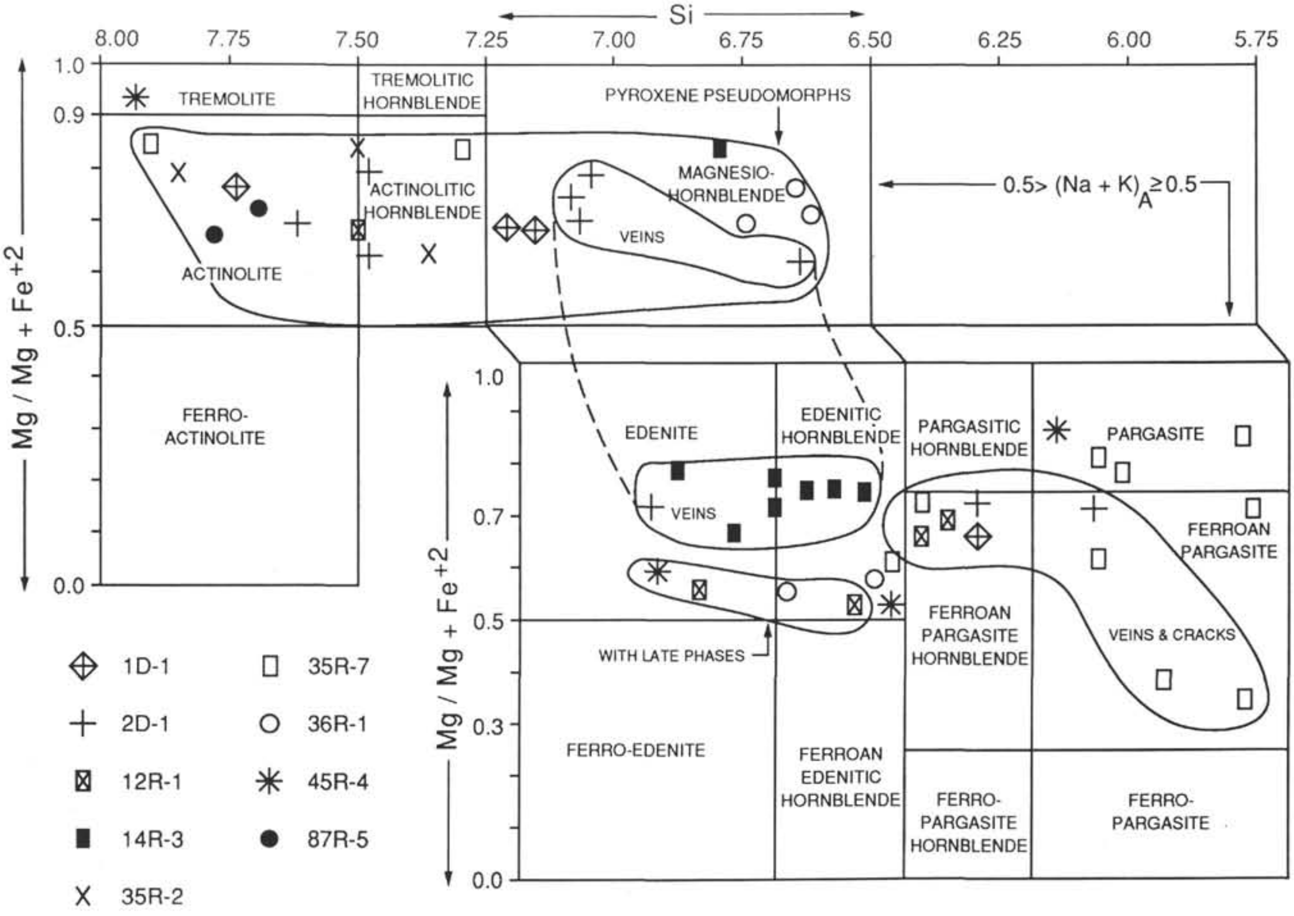

Figure 2. Distribution of calcic amphibole compositions from Hole 735B. Amphibole nomenclature is after Robinson et al, 1982. Most aluminous pargasite and pargasitic hornblende was found in cracks, veins and replacing deformed igneous phases in gneissic gabbros. Large vein amphiboles compositions vary from edenitic to magnesio-hornblende, depending on assumptions for recalculation of formula. Actinolite and actinolitic hornblende were common replacements of cores of clinopyroxene porphyroclasts and foliation planes of secondary pyroxene. Hornblendes "with late phases" were observed with apatite and zircon in ferrogabbro. Abbreviations used for the following samples: 1D-1=Sample 118-735B-1D-1, 26-30 cm, Pc. 4; 2D-1= Sample 118-735B-2D-2, 36-39 cm, Pc. 6; 12R-1= Sample 118-735B-12R-1, 65-68 cm, Pc. 5d; 14R-1= Sample 118-735B-14R-3, 31-35cm, Pc. 2A; 35R-2= Sample 118-735B-35R-2, 105-108 cm, Pc. 4g; 35-7=Sample 118-735B-35R-7, 14-17cm, Pc. 2; 36R-1=Sample 118-735B-36R-1, 17-20, Pc. 3; 45-4= Sample 118-735B-45R-4, 136-140, Pc. 7; 87-5= Sample 118-87R-5, 20-22, Pc. 3.

sodic plagioclase, analcime, or thomsonite (Table 8; Pl. 1, Fig 6). The maximum temperature indicated by the presence of analcime is 200°C (Liou, 1971). Chlorite replaced plagioclase and occurs in a trellis texture with magnetite rods (Sample 118-735B-37R-2, Pc. 1H, 113–117 cm) or with Fe-sulfide and ilmenite (Sample 118-735B-45R-4, Pc. 7, 136–140 cm) forming pseudomorphs. Needles of actinolite replaced the diopside. Ilmenite has been replaced by abundant sphene and scattered grains of golden brookite (e.g., Sample 118-735B-70R-2, Pc. 2, 8–10 cm). Sphene was observed in a trellis texture with ilmenite or intergrown with diopside. Large, pink, euhedral sphene crystals are also present. These zones frequently contain trace amounts of chlorine-bearing apatite, which may have been of magmatic origin originally, but now appears metamorphic (see Vanko and Stakes, this volume). There are large euhedral Fe-sulfides in Core 118-735B-45R. Diopside is increasingly abundant in the lower 25% of the core, both within the breccia zones and within the small vein networks that extend into adjacent host rock from these zones.

Veins

The vein diopside was found as euhedral barrel-shaped grains, surrounded by a matrix of chlorite, in segregated veins with sodic plagioclase and lesser amounts of epidote and sphene, or in monomineralic veins cutting a host variably replaced by diopside or amphibole. Textural relationships suggest that the chlorite matrix in the former setting is a replacement of earlier plagioclase and is not contemporaneous with the diopside. Epidote occurs both as euhedral crystals and as replacement of vein plagioclase. Calcite also appears in very oxidized veins, probably as a replacement of plagioclase or epidote. Diopside and calcite were intergrown in a trellis texture in one sample, and we inferred that the carbonate was a late replacement of plagioclase or epidote. Analcime veins are characteristically full of actinolite inclusions, suggesting a replacement of earlier sodic plagioclase. In at least one sample, epidote was found similarly filled with actinolite fibers.

Minerals of Ambiguous Origin

Before discussing the controls on the distribution of metamorphic minerals, we need to point out the significance of some mineral phases that are of ambiguous origin (magmatic vs. secondary) or are unexpected in oceanic gabbros. An association of incompatible element-rich minerals, such as zircon, phlogopite, apatite, sphene, and carbonates, was

Table 7. Mica, chlorite, and talc compositions from metamorphosed gabbros and late magmatic intrusions, Hole 735B.

Analysis	1	2	3	4	5	6	7	8	9	10	11	12	13	14	15	16
SiO_2	36.11	37.75	35.90	38.18	37.98	37.20	65.63	26.43	26.89	40.21	35.39	34.38	37.55	34.75	62.73	30.42
TiO_2	3.71	0.11	0.04	0.09	0.18	0.05	0.01	0.03	0.00	2.36	0.585	0.44	0.37	0.00	0.01	0.03
Al_2O_3	13.84	15.65	18.96	16.17	16.97	18.57	0.246	19.50	19.94	14.851	15.92	17.17	14.44	17.75	0.34	20.02
FeO*	19.84	14.64	12.07	13.43	15.22	14.80	2.50	24.59	26.25	9.22	23.65	24.59	21.89	24.10	4.38	12.15
MnO	N.D.	0.08	0.07	0.11	0.10	0.11	0.00	0.53	0.79	0.05	0.22	0.192	0.137	0.23	0.03	0.10
MgO	12.28	16.71	19.42	18.88	17.18	18.77	30.76	16.21	15.88	21.18	9.87	9.41	12.85	10.39	28.10	27.39
CaO	0.06	0.02	0.02	0.04	0.00	0.00	0.01	0.03	0.08	0.00	0.334	0.00	0.013	0.01	0.00	0.03
Na_2O	0.39	0.35	0.12	0.32	0.81	0.51	0.13	0.07	0.04	0.17	0.16	0.09	0.22	0.09	0.09	0.02
K_2O	8.82	8.35	7.97	7.93	8.38	7.01	0.02	0.03	0.05	7.33	8.49	8.30	8.94	8.66	0.02	0.05
Cl	N.D.	N.D.	0.02	0.08	0.14	0.01	0.00	N.D.								
Sum	94.68	93.64	96.55	95.22	97.10	97.02	99.30	87.43	89.94	95.75	95.01	95.06	96.81	96.41	95.74	90.19
Si	5.557	5.679	5.516	5.542	5.361	8.030	5.577	5.557	5.717	5.545	5.406	5.709	5.371	7.303	5.537	
Ti	0.428	0.120	0.005	0.010	0.020	0.004	0.001	0.004	0.000	0.253	0.069	0.052	0.042	0.000	0.013	0.004
Al	2.512	2.776	3.433	2.795	2.917	3.151	0.035	4.849	4.858	2.488	2.939	3.182	2.587	3.234	0.338	4.295
Fe	2.508	1.842	1.551	1.648	1.858	1.783	0.256	4.340	4.573	1.096	3.098	3.233	2.783	3.116	4.379	1.850
Mn	N.D.	0.010	0.009	0.014	0.012	0.015	0.000	0.095	0.139	0.006	0.029	0.026	0.018	0.030	0.027	0.016
Mg	2.818	3.747	4.448	4.129	3.736	4.031	5.610	5.099	4.890	4.488	2.305	2.206	2.913	2.393	4.876	7.431
Ca	0.010	0.003	0.002	0.007	0.000	0.000	0.002	0.006	0.017	0.001	0.056	0.000	0.002	0.001	0.032	0.000
Na	0.116	0.102	0.036	0.091	0.228	0.144	0.032	0.030	0.018	0.046	0.050	0.030	0.065	0.027	0.090	0.006
K	1.732	1.599	1.562	1.485	1.560	1.288	0.002	0.009	0.013	1.329	1.697	1.666	1.734	1.707	0.017	0.012
Catsum	15.683	15.771	16.562	15.780	15.874	15.777	13.969	20.012	20.030	15.457	15.789	15.800	15.854	15.879	12.684	19.152

NOTE: All formulas were based on 22 oxygens, except as indicated) Analysis 1 and 2 are from Sample 118-735B-2D-1, Pc. 12. This is a ferrogabbro with apatite and zircon. Analyses 1 is magmatic biotite that is present as brown, titanium-rich flakes; Analysis 2 is metamorphic green biotite in the foliation plane. Analyses 4 and 5 are from Sample 118-735B-35R-2, 105–108 cm, Pc. 4G. A deformed zone within this gabbro has been infiltrated by an LMI that contains sodic plagioclase, quartz, diopside, zircon, biotite, apatite, and sulfide. These analyses are of metamorphic phlogopite in the gabbro that was found replacing plagioclase. Analyses 6 and 7 are from Sample 118-735B-35R-7, 14–17 cm, Pc. 2. This is a cataclastic olivine gabbro with extensive hydrous alteration. Analyse 6 is a green phlogopite found intergrown with paragasite in a coronitic replacement of plagioclase. Analyses 7 is a talc found with cummingtonite in an olivine pseudomorph. Analysis 8 is a chlorite that replaces plagioclase in Sample 118-735B-57R-2, 11–18, Pc. 1B (formula based on 28 oxygens). This is a brecciated gabbro with strongly zoned plagioclase and infiltration by LMI. Analysis 9 is a chlorite found in a coronitic replacement of plagioclase in Sample 118-735B-68R-3, 62–64 cm, Pc. 5 (formula based on 28 oxygens). This is primarily composed of a hydrothermal vein with ferro-pargasite, chlorite, epidote, diopside, and sodic plagioclase. Analyses 10 through 15 are from Sample 118-735B-78R-4, 54–59 cm, Pc. 5B. This is an amphibolitized gabbro with ortho-amphibole and magmatic and metamorphic mica that is heavily veined with sodic plagioclase. This latter feature might be an LMI infiltrate. Analysis 10 is brown titanium biotite found along grain boundaries. Analysis 11 is a pale brown replacement of plagioclase. Analysis 12 is a bright green metamorphic phlogopite, while Analyses 13 and 14 are colorless, and fine-grained replacements of plagioclase, respectively. Analysis 15 is a talc observed as a pseudomorph of olivine mixed with phlogopite and pargasite. Analysis 16 is a dark chlorite (sheridanite) found in a vein in Sample 118-735B-82R-7, Pc. 2. Analysis 2 is a phlogopite from the same sample, found as a coronitic replacement of olivine-plagioclase grain boundaries.

observed for the Stillwater and Bushveld complexes, which has been attributed to late magmatic exsolution of a hydrothermal fluid (Boudreau et al., 1986). Minerals of ambiguous origin observed in the Hole 753B gabbros similarly include mica (biotite and phlogopite), brown Ti-amphibole, diopside, apatite, and zircon. Zircon occurs in evolved gabbro or trondhjemite that is intrusive into less-evolved host gabbro. A late felsic pegmatite intruding a deformed olivine gabbro in Unit VII yielded adequate zircon to provide a lead isotope age. Zircon was also observed in small quantities within the Fe-Ti oxide gabbros. The stratigraphic distribution of zircon is provided in Figure 1 (ZR). In many cases, the presence of zircon was verified by the energy dispersive spectra (EDS). This was found throughout the core, but was consistently associated with felsic veins or segregations, which have been interpreted as late magmatic intrusives. The existing literature suggests that zircon may be an ubiquitous, though sparse, magmatic phase for seafloor plutonic rocks of more evolved felsic compositions (e.g., Ito and Anderson, 1983; Engel and Fisher, 1975; Mevel, 1988; Elthon, 1987).

Apatite, mica, diopside, and brown hornblende occur both as magmatic and metamorphic phases within the core. Apatite of definite igneous origin can be seen as clear islands in igneous clinopyroxene in the evolved Fe-gabbros. Magmatic apatite, generally associated with magmatic amphibole and ilmenite, is common in oceanic differentiated gabbros (Prinz et al., 1976; Elthon, 1987; Kelley and Delaney, 1987; Mevel, 1988). Apatite of late magmatic or hydrothermal origin is rich in chlorine and is associated with Cl-rich vein amphiboles (Vanko and Stakes, this volume). It is unclear whether the hydrothermal apatite replaced igneous apatite, or whether this required an external source for the phosphate. Boudreau et al. (1986) similarly argued that the Cl-rich apatite in the Bushveld and Stillwater complexes must have formed from a Cl-rich hydrothermal fluid. Cumulate apatite in these intrusions is not rich in Cl and is frequently more enriched in fluorine. They proposed that this Cl-rich hydrous fluid was deuteric in origin, but that had exsolved from the magma during the last stages of solidification.

A similar dilemma exists for the presence of mica in many of the gabbros. Reddish biotite of magmatic origin (based on texture and composition) is present in the trondhjemite of Core 118-735B-54R and in a ferrogabbro (Sample 118-735B-2D-1, Pc. 12) coexisting with apatite and zircon. This reddish-brown biotite is Ti-rich (Table 7) and may contain traces of fluorine and chlorine (see Vanko and Stakes, this volume). These magmatic biotites can be compared to the compositions of post-cumulus primary phlogopites observed in the Stillwater Complex (Page and Zientek, 1987). The Stillwater phlogopites all contain more than 3 wt% of TiO_2 and are frequently associated with late-stage brown hornblende or as rims on chromite. Green biotite, observed as rims on ilmenite grains in the oxide-rich units of Hole 735B, may have an origin similar to those described for the Stillwater Complex, because some compositional variations of phases in the latter setting were apparently tied to the local assemblage. A similar relationship between biotite and magnetite was observed in the upper zone of the Bushveld Complex, with well-developed phlogopite rims on cumulus magnetite (Boudreau et al., 1986). Green biotite has also been identified as a synkinematic phase in the same sample as the reddish magmatic biotite, occurring as small flakes that are aligned with neoblasts of Ti-hornblende, within planes of foliation in the Fe-Ti oxide-rich gabbros (Pl.

Table 8. Representative analyses of zeolites and epidotes from Hole 735B.

	Zeolites				Epidotes					
	1	2	3	4	5	6	7	8	9	10
SiO_2	57.87	41.01	38.36	45.66	38.89	38.53	39.95	38.26	39.11	39.08
TiO_2	0.00	0.03	0.00	0.02	0.07	0.05	0.03	0.18	0.06	0.06
Al_2O_3	24.19	28.57	29.90	26.57	30.91	27.66	31.64	28.84	29.65	27.95
FeO*	0.16	0.00	0.00	0.00	4.76	7.88	2.98	7.77	5.55	7.87
MnO	0.00	0.14	0.05	0.00	0.08	0.17	0.09	0.15	0.05	0.00
MgO	0.02	0.00	0.00	0.00	0.05	0.03	0.04	0.01	0.04	0.02
CaO	0.41	11.25	12.66	2.24	23.98	22.94	23.37	24.40	23.53	23.40
Na_2O	8.19	4.84	3.89	13.71	0.02	0.02	0.00	0.02	0.00	0.02
K_2O	0.052	0.00	0.00	0.05	0.01	0.00	0.00	0.01	0.01	0.01
Cl	0.00	0.00	0.00	0.05	N.D.	0.00	0.00	0.00	0.00	0.00
Sum	90.91	85.90	85.28	88.35	98.74	97.27	98.10	99.65	98.01	98.42
Si	2.242	6.258	5.935	6.761	6.003	6.144	6.116	5.979	6.101	6.152
Ti	0.000	0.003	0.000	0.002	0.008	0.006	0.003	0.021	0.007	0.008
Al	1.195	5.181	5.455	4.639	5.623	5.197	5.707	5.309	5.451	5.186
Fe	0.006	0.000	0.000	0.006	0.614	1.051	0.382	1.014	0.724	1.036
Mn	0.000	0.018	0.006	0.000	0.064	0.023	0.012	0.021	0.006	0.000
Mg	0.001	0.000	0.000	0.000	0.012	0.006	0.009	0.004	0.008	0.005
Ca	0.018	1.854	2.099	0.355	3.966	3.919	3.832	4.085	3.933	3.948
Na	0.665	1.444	1.167	3.937	0.004	0.005	0.000	0.004	0.000	0.005
K	0.003	0.000	0.004	0.009	0.002	0.000	0.000	0.000	0.001	0.002
Cl	0.000	0.000	0.000	0.004	0.000	0.000	0.000	0.000	0.000	0.000
Catsum	4.312	14.816	14.717	15.709	16.234	16.254	16.027	16.473	16.233	16.344

NOTE: Analysis 1 is from Sample 118-735B-19R-2, 98–100 cm, Pc. 12, a brittlely deformed metagabbro; analcime from a late vein filled with fibers of actinolitic hornblende. Formula is based on 6.5 oxygens. Analysis 2 is thomsonite replacing igneous plagioclase in Sample 118-735B-63R-5, Pc. 4A. Formula is based on 23 oxygens. Analyses 3 and 4 are from Sample 118-735B-63R-6, Pc. 5B. Analysis 3 is thomsonite replacing plagioclase, and Analysis 4 is a natrolite vein. Both formulas based on 23 oxygens. Analysis 5 is from Sample 118-735B-20R-2, 10–13, Pc. 1E, an amphibolitized gabbro cut by plagioclase, An_{28}. All epidote formulas based on 25 oxygens. Analyses 6 and 7 from Sample 118-735R-3R-2, 113–117, Pc. 1H, a hydrothermal breccia. Analysis 6 is an epidote that replaces plagioclase and is intergrown with actinolitic hornblende. Analysis 7 is from a coarse aggregate of epidote. Analysis 8 is from Sample 118-735B-64R-4, 73 cm, Pc. 1H. This is an epidote that replaces plagioclase and is associated with diopside and chlorite. Analyses 9 and 10 are from Sample 118-735B-68R-3, 62–64 cm, Pc. 5. The epidote in Analysis 9 was found intergrown with metamorphic diopside. The epidote in Analysis 10 was found in veins.

2, Fig. 1, Table 7). Brown to green phlogopite (Mg/Fe = 2.8–3.0, see Table 7) typically was found as part of metamorphic coronas that statically replaced margins of olivine and plagioclase (see "Coronitic Replacement" section, this chapter). These two secondary micas are systematically Ti-poor (Table 7), in contrast to the magmatic biotite. Similar to zircon, mica is actually not rare in plutonic rocks, having been reported for gabbros from the Cayman Trough (Ito and Anderson, 1983) and silicic dikelets from the Indian Ocean (Engel and Fisher, 1975).

Magmatic diopside is associated with the trondhjemitic magmas and lower troctolites (see Dick et al., this volume, b, for a description of the Cr-diopside found in the latter setting), while hydrothermal diopside is characteristic of diopside-plagioclase and felsic veins. The diopside observed in the LMIs forms beautiful euhedral greenish crystals, which may have been subsequently amphibolitized (Pl. 1, Fig. 2). Other minerals include albite, zircon, and sparse quartz. The quartz contains aqueous fluid inclusions with a trace of methane, probably derived from a metamorphic source (Vanko and Stakes, this volume). A characteristic assemblage occurs in the vicinity of these late magmatic intrusions and the associated hydrothermal breccias. It includes diopside epidote, actinolite, chlorite, sodic plagioclase, sphene, thomsonite, and brookite (Pl. 2. Fig 2). Textural relationships indicate a sequential crystallization and that the diopside may be fringed with secondary actinolite (Pl. 2., Fig. 3). Diopside may occur as monomineralic vein filling or as aureoles around magmatic augite, when it is then clearly secondary (Pl. 2, Fig 4). Its origin is more problematic where it is associated with sodic plagioclase in leucocratic veins, which texture mimics the texture of the enclosing gabbro. Fluid inclusion and stable isotope compositions, however, suggest a hydrothermal origin (Vanko and Stakes, this volume). Hydrothermal clinopyroxene has been described in the Skaergaard Intrusion (Manning and Bird, 1986); these are systematically depleted in aluminum and enriched in calcium compared to the magmatic pyroxenes, demonstrating crystallization at lower temperatures (Lindsley, 1983). Skaergaard diopsides found in early clinopyroxene-hornblende-biotite veins have had estimated temperatures of formation of 500° to 750°C, while hydrothermal diopsides associated with subsolvus calcic amphiboles have had estimated temperatures of formation of less than 500°C (Bird et al., 1986; 1988; Manning and Bird, 1986).

Diopside compositions for proposed hydrothermal, metamorphic, and magmatic origins are presented in two pyroxene quadrilaterals (Fig. 3) and compared with estimated temperatures from Bird et al. (1986) (Fig. 3C). Figure 3A depicts the range of compositions for pyroxenes that formed during plastic deformation (both orthopyroxene and clinopyroxene) compared to relict clinopyroxene porphyroclasts. Clinopyroxene neoblasts tend to be more diopsidic in composition, presumably reflecting their lower temperatures of formation compared to the relict igneous porphyroclasts. One large porphyroclast was found to be zoned from an augite core to a diopsidic rim (see analyses for Sample 118-735B-56R, Pc. 2B, in Figure 3A). Pyroxene compositions from the LMIs exhibit the same range of compositions as the more Fe-rich neoblasts—supporting the observation that plastic deformation was contemporaneous with the formation of the LMI. The LMI clinopyroxene compositions are more Fe-rich as a result of their more magmatically evolved character. The LMI pyroxene compositions grade into, but do not overlap, the monomineralic vein pyroxene compositions illustrated in Fig-

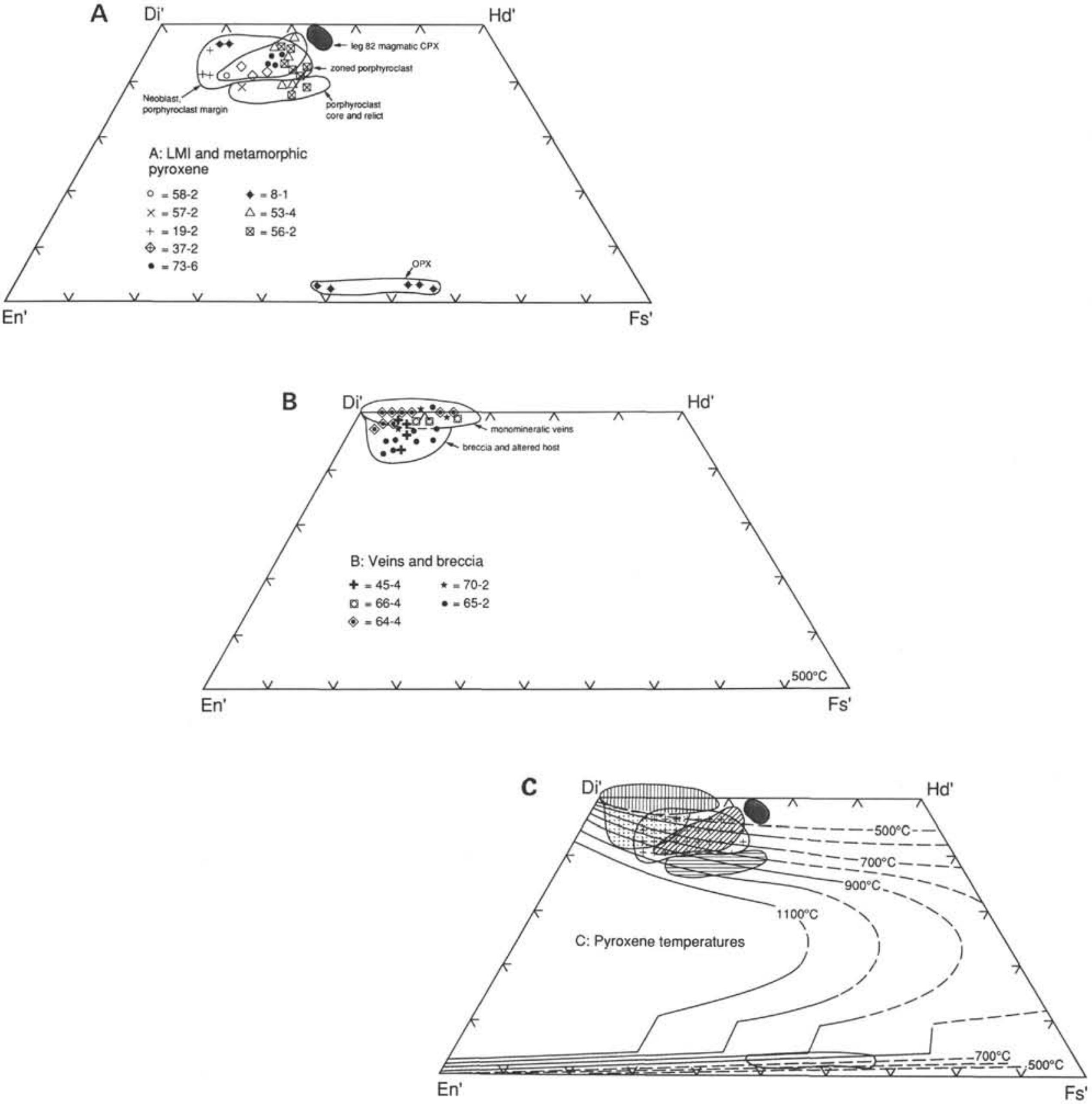

Figure 3. Pyroxene quadrilateral with clinopyroxene compositions. A. Pyroxene in late magmatic intrusions [LML=late magmatic liquid; 53-4 (=Sample 118-735B-53R-4, 5-15 cm, Pc. 1b); 56-2 (=Sample 118-735B-56R-2, Pc. 2b); 73-6 (=Sample 118-735B-73R-6, Pc. 1b), 58-2 (=Sample 118-735B-58R-2, 10-17 cm, Pc. 1B)] compared to clinopyroxene porphyroclast [56-2] and neoblast (19-2, 37-2, 8D-1 (=Sample 118-735-8D-1, Pc. 4) compositions. Compositions for 73-6 include grains in vein as well as in partially resorbed xenocrysts. Compositions for Leg 83 magmatic CPX from Mevel (1982). B. Pyroxene in veins and breccias [45-4 (=Sample 118-735B-45R-4, 136-140, Pc. 7), 65-2 (=Sample 118-735B-65R-2, 18-25 cm, Pc. 1b), 64-4 (Sample 118-735B-64R-4, 73-76 cm, Pc 1h), 66-4(= Sample 118-735B-66R-4, 14-19 cm, Pc. 4), 70-2 (=Sample 118-735B-70R-2, 8-10 cm, Pc. 2)]. C. Pyroxene quadrilateral with temperature estimates, after Bird et al, 1986. Fields for pyroxene groups from Figures 3A and 3B are indicated to show approximate temperature relationships.

ure 2B. The monomineralic veins are consistently Ca-rich, low in aluminum, chromium, and titanium. This diagram shows analyses of the results of a 0.9-cm traverse across an igneous pyroxene crystal crosscut (and replaced by) a diopside vein (see analyses for Sample 118-735B-65R-2, 18–25 cm, Pc. 1B; Fig. 2B). The secondary pyroxene compositions in the altered host rock show a gradient having an increasing diopside component with proximity to the vein. This variation in pyroxene compositions may represent a replacement phenomenon, or more likely, an artifact of a temperature gradient with increasing temperatures of crystallization from the vein to the surrounding host. Clinopyroxene compositions from the hydrothermal breccias show similar variations in composition, suggesting a similar origin of magmatic pyroxenes recrystallizing to metamorphic pyroxenes under local variations in temperature. These observations suggest that the magmatic diopside (= LMI) is more Fe-rich, as well as slightly more Al-rich, than the hydrothermal or replacement diopside and is intermediate in composition between the igneous augite (= gabbro) and the vein diopside. The LMI diopside might be magmatic differentiates of the igneous augite; the vein diopsides are clearly metamorphic, which is consistent with their ^{18}O compositions (Vanko and Stakes, this volume, and Table 1). The pyroxenes in the breccia represent a suite of compositions that includes both vein and LMI types, suggesting that some of the pyroxene may have been derived from an LMI-type source that was subsequently replaced by a hydrous fluid and exhibited extensive vein-type replacement. This distinction does not preclude a magmatic source for part of the hydrous fluids percolating in the cracks along which the vein diopside forms.

Figure 3C is a pyroxene quadrilateral taken from Bird et al. (1986) upon which estimated pyroxene isotherms have been projected. We have superimposed onto these isotherms the fields for our different types of pyroxenes. The relict pyroxene porphyroclasts represent temperatures of 1000° to 800°C; neoblasts represent temperatures from 1000° to below 500°C; LMI pyroxenes range in temperature from 900° to below 500°C; pyroxenes from breccias and heavily veined rocks are intermediate in composition between LMI and vein pyroxenes, with estimated temperatures of 900° to 500°C, and the veins all plot within the lowest temperature portion of the composition space at temperatures at or below 500°C. The secondary diopsidic pyroxene, whether from an LMI or plastic deformation, is much more resistant to hydrous replacement than other mafic phases. Some of the overlap in the range of compositions thus may be the result of artifacts of previous metamorphic episodes. However, these results do show a variation in the range of clinopyroxenes that is consistent with both magmatic and hydrothermal origins.

Both deformed and undeformed gabbros contain relatively high volumes of reddish brown Ti-pargasitic hornblende. Intercumulus brown aluminous hornblende is clearly of magmatic origin, suggesting that some of the melts were hydrous. Brown hornblende of similar Ti-rich (pargasitic hornblende) composition appears as rims on or exsolution blebs in clinopyroxene (Pl. 2, Fig. 5) symplectically intergrown with clear clinopyroxene, and as neoblasts with clinopyroxene and ilmenite in foliated rocks. These textural associations and compositions are consistent with post-cumulus pargasite and pargasitic hornblende observed in the Stillwater Complex and described by Page and Zientek (1987). These latter hornblendes all contain 11%–12% Al_2O_3 and 2%–3% TiO_2, and have estimated temperatures of formation of 905° to 981°C. The quantity of synkinematic brown pargasitic hornblende and the fact that it increases in abundance with increasing deformation in the Hole 735B gabbros argues against a purely magmatic source; however, there is no obvious break in optical properties or chemical compositions on which to distinguish separate populations. It is possible that small quantities of seawater were present to stabilize brown hornblende during the highest-temperature deformation episodes, but the Ti-pargasite is not characteristically Cl-rich as are the Fe-pargasites in the synkinematic veins. The association of the Ti-pargasite with sub-solidus features is apparent on a thin-section scale. For example, in Sample 118-735B-78R-3 (110–119 cm) a hornblende-plagioclase vein crosscuts an undeformed gabbro. Intergrown red-brown Ti-pargasite and metamorphic clinopyroxene, similar to the synkinematic phases described above, are present along the margins of the vein and line small cracks in the igneous augite. This association of red-brown hornblende with veining supports an origin of external fluid for at least some of the observed occurrences.

OXYGEN ISOTOPE DATA

Fresh mid-ocean ridge basalt has a $\delta^{18}O$ composition of about 5.8‰ (Taylor, 1968; Muehlenbachs and Clayton, 1976; Ito et al., 1987). Gabbroic cumulates that have not interacted with an external reservoir of fluid would be expected, on average, to have this bulk isotopic composition. Small variations in whole-rock $\delta^{18}O$ may result from variations in modal compositions, as plagioclase tends to be more isotopically enriched in the heavier isotope (e.g., have a few tenths per mil higher value for $\delta^{18}O$) than either clinopyroxene or olivine at isotopic equilibrium at magmatic temperatures or after a period of sub-solidus isotopic exchange. Similarly, oxides tend to concentrate the light isotope, and the oxide-rich gabbros also would be expected to have a lighter primary value for $\delta^{18}O$. Fresh seawater has a $\delta^{18}O$ composition of zero, and magmatic water is assumed to have a $\delta^{18}O$ value of 6 to 8‰ (Boettcher and O'Neil, 1980; Taylor, 1977; Craig and Lupton, 1976; Shepherd, 1986), with the heavier values associated with extensive magmatic differentiation. Large modifications of the whole-rock $\delta^{18}O$ composition can result from seawater-gabbro interactions, and the final composition of the rock reflects both the temperature and the water-to-rock ratio (Taylor, 1977, 1984; Ito and Clayton, 1983). At temperatures above about 225°C, exchange between seawater and crustal rocks (or replacement by secondary phases) will deplete the rocks of ^{18}O, whereas exchange or replacement at lower temperatures (e.g., formation of smectite) will enrich the rocks in ^{18}O. Some minerals rich in SiO_2 (e.g., quartz, analcime, prehnite, thomsonite) are especially rich in ^{18}O, and their presence will also result in an isotopic enrichment compared to fresh gabbro, even at moderate temperatures.

A complicating factor is the possibility of magmatic fluids playing an important role in some discrete horizons. Progressive magmatic differentiation should result in primary plagioclase and pyroxene compositions of 6.2 to 6.4‰ and 5.5‰, respectively (Dunn, 1986). Equilibration with a high-temperature aqueous phase of magmatic oxygen isotopic composition (5–6‰) might result in isotopic compositions that are slightly depleted in ^{18}O (see Mathews et al., 1983; Dunn, 1986). A second complicating factor is that under conditions of low water-to-rock ratios, the hydrothermal fluid will evolve in isotopic composition, becoming progressively enriched as the rock is depleted in ^{18}O. Evolved fluids may be several mils heavier in ^{18}O than fresh seawater, depending on the amount of rock with which it has exchanged, and may become isotopically indistinguishable from magmatic or deuteric fluids or a mixture of these and hydrothermal fluids. Horizons that include phases previously associated with late magmatic or hydrous fluids could contain evidence of such processes. Detailed analyses of mineral separates and phase chemistry, in conjunction with fluid inclusion studies, are required to assess the role of magmatic fluids or mixtures of magmatic and hydrothermal fluids (see Vanko and Stakes, this volume, for a detailed discussion).

The isotopic profile produced on whole-rock powders is presented in Figure 1, and data are presented in Table 1. Values of whole-rock powders varied from 2.9 to 7.0‰, with 65% of the core showing depletions in ^{18}O from a normal value of 5.8‰, which must result from interaction with seawater at moderate to high temperatures. Horizons that are depleted in ^{18}O occur primarily in the upper structural domain and the breccia horizons of Units IV and V, but isotopic depletions are also conspicuous down to the bottom of the core. This indicates that seawater must have penetrated several kilometers into the crust while it remained at high temperatures. The distribution of ^{18}O-depleted zones suggests the mechanism and timing of this seawater penetration. From 0 to 180 mbsf, the rocks in the core are pervasively depleted in ^{18}O to values as low as 3.5 ‰. From 200 to 350 mbsf, isotopic compositions reflect highly variable but conspicuous ^{18}O-depleted compositions that are associated with the breccia zones. Below 350 mbsf, most samples have an isotopic composition near igneous, with depleted values conspicuous in the bottom 50 m.

Rocks that contain the magmatic/hydrothermal assemblage were primarily found between Cores 118-735B-56R and 118-735B-76R, although smaller brecciated and recrystallized intervals were found in Cores 118-735B-37R-2 and 118-735B-45R-4. Isotopic whole-rock values near these horizons have normal or heavy values of $\delta^{18}O$. These are approximately 15 cm wide and occur in a region of rapid changes in igneous mineral size and apparent mixing between Fe-Ti gabbro and olivine-rich gabbro. Veins in Cores 118-735B-43R to 118-735B-44R and adjacent to this oxide-rich zone similarly contain clinopyroxene, sodic plagioclase, actinolite, sphene, and chlorite (e.g., 118-735B-43R-1, 126–128, Pc. 15; 118-735B-44R-4, 135–139, Pc. 8B). The first of these examples has not been depleted in ^{18}O, while the last has been (see Table 1). These shallow breccia horizons may have been altered by isotopically enriched metamorphic fluids that discharged from adjacent metamorphosed host or the isotopic compositions may be the artifact of localized hydrous magmatic fluid.

Isotopic depletions correlated with breccia horizons are conspicuous in Cores 118-735B-56R to 118-735B-60R, 118-735B-64R, 118-735B-67R, and 118-735B-70R. For these horizons, the depletions are associated with isotopically light hydrothermal plagioclase, diopside, chlorite, and epidote. Diopside-plagioclase veins are frequently altered to hydrothermal phases, and these veins are also uniformly depleted in ^{18}O, except possibly in Cores 118-735B-72R to 118-735B-74R. A diopside-plagioclase vein from Core 118-735B-70R formed at a temperature near 500°C from a fluid having a $\delta^{18}O$ value of 3.8‰ (Vanko and Stakes, this volume). A fluid having this isotopic composition might be derived either by mixing magmatic and hydrothermal fluids, as we inferred from the mineralogy and textures, or by a highly evolved hydrothermal fluid.

DISCUSSION

Controls on the Distribution of Metamorphic Minerals

Alteration Index and Its Correlation With Vein Density

During Leg 118, shipboard thin-section descriptions required an estimate of original clinopyroxene and percent replacement by amphibole. We used the percentage (0%–100%) of magmatic pyroxene replaced by secondary amphibole as an alteration index to reflect the total hydrous replacement of the core. The alteration index has been averaged for each core and smoothed by eye, to reflect gradual changes in hydration. This is an appropriate, although approximate, representation because (1) clinopyroxene is present in almost every sample; (2) the replacement of clinopyroxene is generally optically recognizable and relatively consistent among different observers; and (3) coronitic and pseudomorphous replacements provided a consistent and predictable progression of phases with increasing hydration, for which the replacement of clinopyroxene was a ubiquitous component. The minerals present in coronitic replacements of olivine, orthopyroxene, and plagioclase were, with increasing hydration: amphibole (actinolite, tremolite and Fe-Mg amphibole), then chlorite, and finally mica in the most hydrated samples. However, this index does not accurately reflect alteration in the brecciated zones characterized by the development of secondary diopside rather than amphibole. Extensive alteration in this latter setting is reflected by the appearance of chlorite (CHL), epidote (EP) as well as diopside (DIO). Figure 1 shows that the alteration index is highest in the upper part of the core, is low between Cores 118-735B-45R to 118-735B-65R, increases from Core 118-735B-65R to 118-735B-70R, and then is low until the bottom of the hole.

The quantity of veins (Fig. 1) was measured on board ship directly from the cores. These veins vary widely downcore from a maximum of 12/m in the upper half of the core to 1/m or less in the lower portion of the core. Above Core 118-735B-50R, most of the veins are synkinematic hornblende-bearing, with associated vein plagioclase appearing at about Core 118-735B-15R. Diopside-bearing veins unrelated to ductile deformation first appear in Core 118-735B-37R and dominate below Core 118-735B-50R. The abundance of amphibole veins decreases sharply below Core 118-735B-68R. Synkinematic amphibole veins dominate in the upper half of the core, while breccias and the sparse post-kinematic veins dominate in the lower half of the core.

There is a rough correlation between alteration index and vein abundance, which would be improved if only amphibole veins were considered. The only zones for which the index is more than 50% is in the heavily veined upper half of the hole. This suggests that the hydrous alteration is tied more closely to the propagating crack network than to the earlier ductile deformation. This relationship was empirically noted during the shipboard thin-section descriptions—if there were no evidence of healed microcracks cutting the sample, then there were no secondary hydrous minerals (Shipboard Scientific Party, 1989). The abundance of crosscutting hornblende veins is related to the extent of ductile deformation, being most abundant in zones with type I through type III textures (foliated to gneissic). The vein network apparently does not crosscut many of the mylonitic zones. The quantity of coronitic and pseudomorphous replacement minerals is also reflected in the alteration index as well as the abundance of amphibole replacing pyroxene downcore. Thus the bulk hydrous alteration, at least in the upper portion of the core, can be associated with the syn-kinematic veins.

Synkinematic Assemblages and Their Correlation With Textural Type

A PX-HB-PLAG assemblage was found in more than 50% of the deformed samples from Cores 118-735B-1D to 118-735B-56R and in 75% of the samples from Cores 118-735B-77R to 118-735B-87R. The distribution of this assemblage is directly associated with the highest grades of deformation, characteristically found with textural types IV and V. The HB-PLAG and ACT HB-NA- PLAG assemblages are found in abundance only in the upper parts of the core. It is clear from Figure 1 that the HB-PLAG and ACT HB-NA-PLAG synkinematic assemblages are present only in areas that have abundant veins. This relationship suggests that while some zones were still undergoing ductile deformation, intervening zones were failing brittlely to form the crack and vein network.

Contrasting Styles of Metamorphism (and Deformation)

We postulate that the permeability created by brittle failure (veins and breccias) of the rocks is responsible for the hydrous metamorphic recrystallization. During synkinematic metamorphism, the synkinematic veins serve as pathways for seawater to penetrate the crust while it is still being ductilely deformed, resulting in hydrous synkinematic assemblages.

The late- to post-kinematic static alteration resulted in coronitic or pseudomorphous replacements that ultimately reflect the initial modal composition. Primary lithology is important in metamorphic stratigraphy in three ways. First, if olivine or orthopyroxene are present, then the hydrous replacement assemblage will include talc, magnetite, an Fe-Mg amphibole, and commonly, mica and chlorite. The absence of this assemblage reflects primary mineralogy, not metamorphic conditions. Second, primary lithology is a control on the secondary phase composition. Metamorphic phases from the ferrogabbros (e.g., mica and hornblende) were more enriched in iron compared to the same phases in the olivine gabbros. This also suggests that primary lithology, not variable metamorphic conditions, controls the phase chemistry on a local basis. Hornblende ± plagioclase veins and associated hydrous alteration dominate the metamorphism in the upper portion of the core (upper and middle structural domains) and the very bottom (lower structural domain). In the lower portion of the core diopside ± plagioclase dominate in heavily veined and brecciated zones.

Lower temperature metamorphism has been restricted to the permeable breccia zones, possibly created by magmatic hydrofracture and resulting from the infiltration of the LMI. Veins in the lower 260 m of the core, and especially in the relatively undeformed regions, characteristically contain diopside, rather than hornblende, and are most abundant proximal to breccia zones. Secondary mineral assemblages within the breccia zones represent temperatures down to zeolite facies. Fluids associated with the breccia zones are apparently the source of minerals in the post-kinematic set of veins.

Timing and Temperature

Plastic Deformation and Synkinematic Veins

In most of the thin sections studied, neoblasts of orthopyroxene occur around porphyroclasts of orthopyroxene, and the same is true for the clinopyroxene. When ortho- and clinopyroxenes are separated by large plagioclase crystals, they likely represent distinct microchemical domains. Neoblasts of orthopyroxene and clinopyroxene in contact were observed in only two samples. For these rocks, equilibrium temperatures were calculated using Wells' (1977) geothermometer. The temperatures calculated are 894° to 908°C for Sample 118-735B-8D-1, Pc. 4 (Table 2); and 849° to 852°C for Sample 118-735-46R-3, Pc. 2B. These temperatures are consistent with dry granulite facies and demonstrate that shearing began as soon as the gabbros were solidified.

A comprehensive discussion of amphibole composition and nomenclature is provided in Vanko and Stakes (this volume), and a compilation of amphibole compositions can be found in Figure 2. The brown magmatic amphiboles found as intercumulus phases, blebs, and lamellae in clinopyroxene and neoblasts are pargasite or Mg-hastingsite. These red-brown amphiboles are stable up to magmatic temperatures. The brown to green hornblende in the high-temperature synkinematic phases similarly is pargasitic to magnesio-hornblende. Temperatures of formation can be estimated for these phases based on Na distribution between the amphibole and coexisting plagioclase. Using this geothermometer, temperatures of formation for the synkinematic veins are approximately 400° to 650°C (Spear, 1982). The amphibole characteristic of the moderate-temperature synkinematic assemblage is actinolitic hornblende and represents lower temperatures. Amphibole that fills cracks created by these deformation episodes compositionally overlaps the synkinematic assemblages in the same sample. Actinolite and tremolite occur as hydrous replacements of olivine and clinopyroxene (Pl. 1, Fig. 4). Talc, anthophyllite, and cummingtonite are also ubiquitous replacements of olivine. These syndeformational to late-deformational assemblages represent temperatures of 500° to 700°C (Vanko and Stakes, this volume). The paucity of greenschist facies minerals within the upper half of the cores suggests that the synkinematic crack network was effectively sealed while metamorphic temperatures were still elevated. Temperatures of formation for plagioclase in the synkinematic veins and adjacent rock wall can be calculated from oxygen isotopic compositions using the equilibrium fractionation between plagioclase and water (O'Neil and Taylor, 1967). For the purpose of this estimate, an intermediate plagioclase composition (An_{30}) and fluids of 0‰ (normal seawater) and 2 ‰ (isotopically shifted hydrothermal fluid) were used. Temperatures for plagioclase formation or isotopic equilibration thus calculated were 350° to 475°C (seawater) and 450° to 650°C (2‰, fluid). These provide minimum estimates for temperatures at which the crack networks were sealed by the formation of the vein minerals.

Veins and Breccias

Structures Related to LMIs

The last column in Figure 1 summarizes the distribution of zircon (ZR) and leucocratic veins (LCV) as well as the "static" metamorphic phases not represented by the alteration index. These assemblages were determined from observed thin sections, which explains the discontinuous pattern. The distribution of zircon is the best indicator of LMI or evolved gabbro. This phase is abundant in Unit I and the upper part of Unit II, but disappears in Core 118-735B-18R near the boundary with a metamorphosed microgabbroic dike. Zircon is scattered in small cataclastic zones in Cores 118-735B-26R to 118-735B-27R. Zircon is present in leucocratic veins and hydrothermal zones in Cores 118-735B-32R to 118-735B-36R, 118-735B-45R to 118-735B-46R, 118-735B-50R and 118-735B-54R. Zircon and the leucocratic veins are especially abundant in the breccia zones in Cores 118-735B-55R to 118-735B-60R and 118-735B-64R-118-735B-69R. The lowest appearance of zircon is in Core 118-735B-74R, although the leucocratic veins appear down to Core 118-735B-79R. We infer from this distribution that the brecciated horizons and associated hydrothermal zones are linked with the late injection of the LMI, even when zircon is not observed in the assemblage.

Structures Not Related to LMIs

Chlorite (CHL) is present as a magnesian variety in coronitic replacements of olivine and plagioclase (Table 9). It is mainly widespread in brecciated zones, where it is greener and richer in iron. Secondary sodic plagioclase (PLG) is in veins with amphibole, but, similar to chlorite, is more closely associated with leucocratic veins and hydrothermal breccias in the lower half of the core. Epidote, diopside, and sphene consistently appear in association with the leucocratic veins and hydrothermal breccias, although not systematically. The host for the microgabbro dike in Core 118-735B-18R and the dike itself, for example, has been altered to epidote, chlorite, and actinolite, and veins contain carbonate and analcime. This boundary is the shallowest occurrence of true greenschist and zeolite facies minerals. Similar local zones of greenschist alteration, indicated by the combined occurrence of chlorite and epidote, are present from this horizon to the bottom of Unit II. Near the boundary between Unit III and throughout Unit IIIA, one sees leucocratic veins and host rock that have been pervasively replaced by hydrothermal epidote, chlorite, sphene, and diopside. These assemblages occur sporadically

Table 9. Representative olivine analyses from metagabbros from Hole 735B.

Analysis:	1	2	3	4	5
SiO_2	37.98	37.46	35.76	33.40	38.36
TiO_2	0.00	0.00	0.00	0.00	0.00
Al_2O_3	0.01	0.01	0.00	0.00	0.00
Cr_2O_3	0.00	0.00	0.00	0.00	0.01
FeO*	22.34	22.19	32.06	50.53	23.29
MnO	0.28	0.29	0.88	1.01	0.37
MgO	40.44	40.12	32.22	15.49	39.20
CaO	0.00	0.00	0.01	0.05	0.03
Sum	101.13	100.15	100.93	100.47	101.28
Si	0.979	0.975	0.972	1.004	0.990
Ti	0.000	0.000	0.000	0.000	0.000
Al	0.000	0.000	0.000	0.000	0.000
Cr	0.000	0.000	0.000	0.000	0.000
Fe	0.481	0.483	0.729	1.271	0.503
Mn	0.006	0.006	0.020	0.026	0.008
Mg	1.553	1.557	1.306	0.694	1.508
Ca	0.000	0.000	0.000	0.002	0.001
Catsum	3.021	3.024	3.027	2.996	3.010
FO	76.1	76.1	64.2	34.9	75.0

NOTE: All formulas were calculated on the basis of four oxygens. Analyses 1 and 2 are from Sample 118-735B-8D-1, Pc. 4. Analysis 1 is an olivine prophyroclast, and Analysis 2 is a neoblast. Analysis 3 is from Sample 118-735B-35R-7, Pc. 2 (14–17 cm). This is a foliated metagabbro having extensive static alteration. Analysis 3 is an olivine having poorly developed, metamorphic, grain boundaries that has been partially replaced by a mixture of cummingtonite, talc, and magnetite, and having grain margins with plagioclase that are replaced by pargasite and phlogopite. Analysis 4 is from Sample 118-735B-56R-2, Pc. 2B (18–22 cm). This is a deformed ferrogabbro with orthopyroxene, clinopyroxene, sodic plagioclase, and abundant apatite, in addition to the Fe-rich olivine. Analysis 5 is from Sample 118-735B-82R-7, Pc. 2 (21–29 cm) and is an undeformed olivine gabbro having extensive coronitic replacements. This olivine was partially replaced by tremolite, with phlogopite, actinolite, and edenitic hornblende along margins with plagioclase.

in Subunit IIIB through Unit IV and are dominant in Unit V and the upper part of Unit VI.

Zones of zeolite grade alteration (ZEO) are indicated by analcime, prehnite, or thomsonite. The lowest temperature alteration, carbonate, and smectite in veins and adjacent host rock, is indicated on the vein histogram. The distribution of carbonate veins, which distinguishes the presence of low-temperature oxidative alteration, is also related to the breccia zones. A very large carbonate and smectite vein occurs in Core 118-735B-38R, and the adjacent rock is highly oxidized to a bright red. The large breccia zones are commonly stained bright red with Fe-oxide, and this oxidation extends into the adjacent intact gabbro. Zeolite-grade minerals as well as the late carbonate-smectite veins show a similar stratigraphic distribution with the greenschist-grade hydrothermal minerals.

This distribution of "static" assemblages demonstrates the absence of correlation with depth. The main characteristic is the association of particular minerals with the hydrothermal brecciated zones: diopside, epidote, chlorite, albite, zeolites and carbonates. It is only in these zones that widespread greenschist facies (chlorite-albite-epidote) and zeolite facies (thomsonite, analcime) assemblages are present. This suggests that when temperature decreased, fluids only circulated in these zones.

Controls on Oxygen Isotope Compositions

Correlation Between ^{18}O Depletions and Veins

It is apparent from Figure 1 that the oxygen isotope profile and the alteration index vary consistently (especially in the upper half of the core), suggesting that isotopic depletions can be correlated with hydrous alteration. Figure 4 is a plot of whole-rock $\delta^{18}O$ vs. alteration index that illustrates this correlation. This correlation would be improved if the hydrothermal breccias rich in diopside were not considered, since in these horizons the extent of seawater modification does not result in a replacement of pyroxene by amphibole. A comparison of the histogram of vein abundances (Fig. 1) with the $\delta^{18}O$ suggests a mechanism for the penetration of seawater. The lowest values of $\delta^{18}O$ are associated with the greatest concentration of synkinematic hornblende veins.

The correlation of ^{18}O-depletions, hornblende vein abundance, and alteration index confirms that seawater penetrated into the lower crust via the synkinematic crack network. Because the synkinematic crack network formed as the last phase of dynamic metamorphism, most of the water penetrated after the high-temperature ductile phase. The lower values of $\delta^{18}O$ for samples near the shallow ductile fault (Core 118-735B-5R to 118-735B-6R) compared to the lower ductile

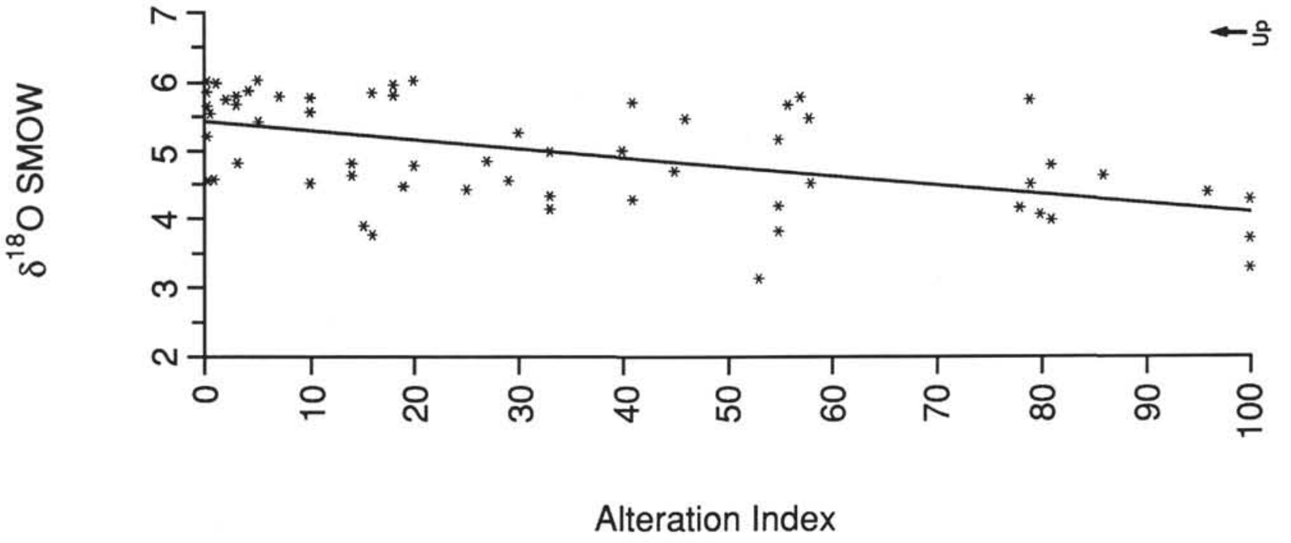

Figure 4. Plot of Alteration Index vs. whole-rock values of $\delta^{18}O$. The Alteration Index was calculated from shipboard thin section descriptions and is the percentage (from 0%–100%) of igneous clinopyroxene replaced by secondary amphibole.

fault (Cores 118-735B-77R to 118-735B-87R) suggest that less water penetrated the lower ductile shear zone. The mylonite from Core 118-735B-6D (e.g., 118-735B-6D-1, 71–74 cm) has a $\delta_{18}O$ value near igneous, although the plagioclase is extensively recrystallized and synkinematic brown amphibole is abundant. This further suggests that the large depletions in ^{18}O were not associated with the high-temperature ductile deformation, but rather with the penetration of the hornblende veins and associated hydrous replacement. We suggest that the extent of recrystallization of the clinopyroxene to amphibole during the dynamic metamorphism reflects the availability of seawater. Apparently, the quantity of water available during ductile deformation was much lower as the middle and lower structural domains developed. That is, seawater was locally abundant during deformation only in the upper structural domain. This is consistent with the distribution of the synkinematic metamorphic assemblages: the HB-PLAG and ACT HB-PLAG assemblages are abundant only in the upper structural domain, where abundant seawater penetrated. The penetration of seawater into the middle structural domain was much more localized and apparent in the lower structural domain only in Core 118-735-87R.

The predictability of the metamorphic phases associated with ductile deformation and the similarity in amphibole composition between veins and hydrous replacement suggest a temperature range limited to mid-to-upper amphibolite grade. At these temperatures, for water-to-rock ratios less than unity, the final isotopic composition of the bulk rock probably reflects variations in the water-to-rock ratio, rather than variations in temperature. That is, under low water/rock conditions ($W/R<1$), the observed final $\delta^{18}O$ composition of the rock was limited by the availability of an isotopically different fluid with which to equilibrate, rather than being a reflection of the temperature of fluid-rock interaction. The crosscutting vein networks, of course, could have a much higher effective value of water/rock ratio than their host rock. Many of the bulk rock powders, especially from the top 180 m of core, were samples cut by networks of small amphibole veins, and can be considered averages of host and vein. Samples showing the most extensive isotopic depletions in the upper 180 m of the core are those having extensive coronitic or pseudomorphous replacement, especially samples containing chlorite, plagioclase, and amphibole, which are isotopically very light. Petrographic study suggests that outside of the brecca horizons, chlorite is present in the samples with the most extensive hydrous replacement, but not in enough abundance to control the isotopic composition. However, the presence of chlorite is indicative of greater quantities of fluid available during static replacement, previously correlated with the abundance of the late-kinematic vein network. Isotopic compositions of mineral separates of plagioclase and amphibole from a subset of these depleted gabbros suggest that the exchange/replacement of plagioclase and the formation of green amphibole control this isotopic profile for the upper half of the core. Samples that are the most ^{18}O-depleted also contain the lightest plagioclase and amphibole contents.

Water-to-Rock Ratios

The relationship between water-to-rock ratio, temperature, and plagioclase isotopic composition for seafloor systems was discussed in Stakes and O'Neil (1982) and Gregory and Taylor (1981), based on models proposed by Taylor (1977). We have used the plagioclase-water fractionation to estimate water-rock ratios. This relationship (plagioclase-water) can be used for gabbros because (1) plagioclase exchanges about five times faster than pyroxene or olivine (Gregory and Criss, 1986); (2) clinopyroxene or olivine are replaced by hydrous minerals (especially amphibole) that are presumably in isotopic equilibrium with the exchanged plagioclase and (3) other phases (chlorite, epidote, sphene) only play a volumetrically important role in the breccia zones and associated veins, which are discussed separately from the altered gabbros.

The relationship between the water/rock ratio, temperature of isotopic exchange, and the final oxygen isotopic composition of basaltic rocks can be approximated by the equation governing the isotopic exchange of plagioclase (An_{30}) (see Fig. 2 in Stakes and O'Neil 1982). Based on this approximation, for gabbroic rocks altered by seawater at temperatures between 400° to 500°C, the final isotopic composition of the rock should be no greater than 4‰ for water/rock ratios near unity. Under these conditions, the resulting hydrothermal fluid would be enriched at least 1 to 3‰. Zones within the core for which the effective water/rock ratio was unity or higher are roughly delineated by bulk oxygen isotopic compositions of less than 4‰. Our calculations show that for average temperatures of metamorphism of between 400° and 600°C, the water/rock ratio in much of the core was much less than one. The average whole-rock isotopic composition for the highly deformed upper structural domain (0–172 mbsf) is 4.5‰; the average for the middle structural domain (172–272 mbsf) is 5.5‰, and the average for the lower structural domain (403–500 mbsf) is 5.7‰—indistinguishable from fresh gabbro. At a median temperature of 500°C, this suggests average water/rock ratios of 0.4 for the upper structural domain and average values of water/rock ratio for the bottom of the core of less than 0.1. Within the upper structural domain, there are also clearly horizons in which the water/rock ratio was near unity, resulting in extensive intervals of highly ^{18}O-depleted compositions.

We suggest that the disappearance of recrystallized clinopyroxene in the syn-kinematic assemblages in the upper and middle structural domains represents availability of seawater during ductile deformation rather than a marked change in temperature. We infer that for these domains there was adequate fluid available during the latter stages of plastic deformation that light brown to green coarse amphibole, rather than pyroxene, was stabilized. The availability of seawater is reflected in the lower average ^{18}O composition of the metamorphosed rocks from these horizons. These data suggest that seawater was pervasively present during the deformation in the upper structural domain and only present in discrete horizons in the middle structural domain. The average whole-rock isotopic composition for the lower structural domain is identical to unaltered rock as a result of the limited availability of seawater. Based on the correlation of ^{18}O and hornblende composition, we suggest that the CPX-HB-PLAG, HB-PLAG, and ACT HB-NA PLAG dynamic assemblages represent high temperature, low water/rock; high temperature, high water/rock; and moderate temperature, high water/rock assemblages, respectively.

SUMMARY AND CONCLUSIONS

The metamorphic stratigraphy of Site 735 is related to (1) shearing and metamorphic recrystallization that began prior to the penetration of seawater; (2) the penetration of seawater via late- to post-kinematic veins and cracks (granulite- to amphibolite-grade metamorphism) or to magmatic/hydrothermal breccias (greenschist to zeolite grade metamorphism). A relationship between hydrous alteration and deformation has been suggested in previous studies of dredged gabbroic rocks (e.g., Ito and Anderson, 1983; Vanko and Batiza, 1982) and is confirmed by the stratigraphic relationships provided by this core. There is no depth-related metamorphism that reflects an increase of temperature along a fixed gradient. Rather, deformation-related metamorphism is dominant in the upper half of the core, while magmatic breccia-related metamorphism is dominant in the lower half of the core. The high initial temperatures of the synkinematic deformation further suggest that the portion of layer 3 recovered in this core was metamorphosed near the axial magma chamber of Southwest Indian Ridge. The results of this study thus provide a model for cooling and hydrothermal alteration of gabbroic rocks at a slow-spreading center, illuminating the role of permeability created by ductile deformation zones in allowing the access of seawater to great depths within Layer 3. Our results suggest that this cooling history and the associated vein mineralization was extraordinarily analogous to what is proposed for the Skaergaard Intrusion, where fluids penetrate along cracks that form at temperatures just beneath subsolidus (Norton et al., 1984). The results of this study indicate:

1. Ductile deformation in the upper half of the core dynamically recrystallized more than 50% of the igneous minerals, with the availability of water controlling the final metamorphic assemblage. Ductile deformation began at temperatures of granulite grade (900°–700°C) and continued to mid-amphibolite grade (to 450°C) with increasing availability of seawater. Where low quantities of seawater were present, the secondary assemblage was modally identical to the primary assemblage, except for the increased abundance of brown amphibole and ilmenite. Increased abundance of seawater produces a modal assemblage in which amphibole, talc, mica, and chlorite replace the mafic phases. The hydrous ductile-deformation assemblage is only abundant in the upper half of the core.
2. Oxygen isotopic compositions of the deformed rocks are similarly controlled by the availability of seawater, and the final $\delta^{18}O$ composition reflects water/rock ratio, rather than temperature. Highly deformed rocks metamorphosed under low water/rock ratios are only slightly depleted from fresh gabbro ($\delta^{18}O$ = 5.8‰). Gabbros deformed under more hydrous conditions are depleted up to 2‰ by high-temperature interactions with seawater. The relationship between deformation and depletions in oxygen isotopes has been previously noted in mineralogically similar gabbros from the Cayman Trough (Ito and Clayton, 1983; Stakes and Vanko, 1986; Stakes et al., 1983).
3. The quantity of hydrous alteration, abundance of amphibole veins, and depletions in oxygen isotopic composition co-vary in the upper half of the core. We conclude from this that seawater is penetrating into the cooling crustal rocks via the permeability created by the deformation episodes. The presence of ductile shear zones thus allows seawater metamorphism to commence at temperatures much higher than those expected in intact crust. The upper half of the core thus represents a "rock-dominated" ($W/R < 1$) seawater hydrothermal system in which permeability has been enhanced by ductile deformation zones.
4. Although horizons of ductile deformation exist in the lower half of the core there are fewer deformation-related veins. As a result, less hydrous replacement is associated with deformation.
5. Metamorphism in the lower half of the core is controlled by seawater penetration into cataclastic zones. These cataclastic zones are characterized by leucocratic veins and felsic intrusions, many of which are zircon-bearing and of magmatic origin. Similar to what has been observed for the Skaergaard Intrusion, we suggest that late magmatic intrusives are contemporaneous with the earliest fractures and may be related to stoping and assimilation. Cataclastic zones are produced by magmatic hydrofracture into horizons where these hydrous, late-magmatic liquids concentrated.
6. Assemblages within the breccia horizons include early diopside and sodic plagioclase, which may be of a late-magmatic or high-temperature hydrothermal origin. Subsequent hydrothermal alteration at greenschist temperatures has replaced sodic plagioclase by epidote and chlorite, ilmenite by sphene, and diopside by actinolite. Continued alteration at zeolite facies temperatures has replaced sodic plagioclase by analcime or thomsonite and sphene by brookite. Continued alteration to ambient seafloor temperatures is reflected in the appearance of late carbonate, smectite, and Fe-oxide sealing fractures.
7. Diopside-hornblende-plagioclase veins that are unrelated to deformation appear to originate from these breccia horizons. Presumably seawater penetrated into these horizons to produce this type of vein, or to metamorphose existing magmatic veins. Clinopyroxene compositions in vein minerals and surrounding altered host rock suggest that the host was still at high temperatures (800° to 600°C) when the cooler fluid penetrated and filled the vein.
8. Oxygen isotopic compositions of breccia horizons are both depleted and normal. The shallower horizons are pervasively depleted in ^{18}O as a result of seawater metamorphism. Deeper portions of the core contain fewer horizons depleted in ^{18}O, even when the rocks are pervasively replaced by hydrothermal minerals. Plagioclase vein minerals are also both depleted and enriched in ^{18}O. This suggests that less seawater has been penetrating to the deeper portion of the core, resulting in hydrothermal fluids that are isotopically enriched. This isotopic enrichment was produced either by exchange with the rocks during metamorphism or by mixing with small amounts of magmatic fluids.
9. The metamorphic stratigraphy from Hole 735B does not resemble the metamorphic stratigraphy commonly found in ophiolites. There is no evidence of pervasive seawater circulation or depletions in oxygen isotopic compositions independent of metamorphic replacement of the gabbro. The penetration of seawater and subsequent metamorphism is controlled not by depth, but by local permeability created by ductile faults or magmatic hydrofracture.

ACKNOWLEDGMENTS

This research was supported by a grant from the ASP-ODP for C. M. and M. C. Support for D. S. and T. C. was provided by JOI/USSAC and by the Ocean Sciences Division of the National Science Foundation. D. S. and M. C. would especially like to thank the Co-Chief Scientists for inviting our participation and A. Adamson for assistance during the cruise. In addition, D. S. would like to thank the coring crew, who sacrificed to her one of their steel balls required to deploy a hard-rock guidebase.

REFERENCES

Batiza, R., and Vanko, D. S., 1985. Petrologic evolution of large failed rifts in the Eastern Pacific: Petrology of volcanic and plutonic rocks from the Mathematician Ridge area and the Guadelupe Trough, *J. Petrol.*, 26:564–602.

Bird, D. K., Manning, C. E., and Rose, N. M., 1988. Hydrothermal alteration of tertiary layered gabbros, East Greenland, *Am. J. Sci.*, 288:405–457.

Bird, D. K., Rogers, R. D., and Manning, C. E., 1986. Mineralized fracture systems of the Skaergaard Intrusion, East Greenland. *Meddelelser om Gronland, Geosci.*, 16:1–68.

Bonatti, E., Honnorez, J., Kirst, P., and Radicati, F., 1975. Metagabbros from the Mid-Atlantic Ridge at 6°N: contact-hydrothermal-dynamic metamorphism beneath the axial valley. *J. Geol.*, 83:61–78.

Boettcher, A. L., and O'Neil, J. R., 1980. Stable isotope, chemical and petrographic studies of high-pressure amphiboles and micas: evidence for metasomatism in the mantle source regions of alkali basalts and kimberlites. *Am. J. Sci.*, 280(A):594–621.

Boudreau, A. E., Mathez, E. A., and McCallum, I. S., 1986. Halogen geochemistry of the Stillwater and Bushveld Complexes: evidence for transport of the platinum-group elements by Cl-rich fluids. *J. Petrol.*, 27:967–986.

Craig, H., and Lupton, J. E., 1976. Primordial neon, helium, and hydrogen in oceanic basalts. *Earth Planet. Sci. Lett.*, 31:369–385.

Dunn, T., 1986. An investigation of the oxygen isotope geochemistry of the Stillwater Complex. *J. Petrol.*, 27:987–997.

Engel, A., and Fisher, R., 1975. Granitic to ultramafic rocks from the Indian Ocean. *Geol. Soc. Am. Bull.*, 96:1553–1578.

Elthon, D., 1987. Petrology of the mid-Cayman Rise spreading center. *J. Geophys. Res.*, 92:658–687.

Fox, P. J., and Stroup, J. B., 1981. The plutonic foundation of the oceanic crust. In: Emiliani C. (ed) *The Oceanic Lithosphere* (*The Sea*: Vol. 7): New York (Wiley), 119–218.

Gregory, R. T., and Taylor, H. P., Jr., 1981. An oxygen isotope profile in a section of Cretaceous oceanic crust, Samail Ophiolite, Oman: evidence for $\delta^{18}O$ buffering of the oceans by deep (>5 km) seawater-hydrothermal circulation at mid-ocean ridges. *J. Geophys. Res.*, 86:2737–2755.

Gregory, R. T., and Criss, R. E., 1986. Isotopic exchange in open and closed systems. *In* Valley, J. W., Taylor, H. P., Jr., and O'Neil, J. R. (Eds.), *Stable Isotopes in High-Temperature Geological Processes. Rev. Mineral.*, 16: Washington (Mineral. Soc. Am.).

Helmstaedt, H., and Allen, J. M., 1977. Metagabbronorite from DSDP Hole 334: an example of high temperature deformation and recrystallization near the Mid-Atlantic Ridge. *Canad. J. Earth Sci.*, 14:886- -898.

Honnorez, J., Mevel, C., and Montigny, R., 1984. Geotectonic significance of gneissic amphibolites from the Vema fracture zone, equatorial Mid-Atlantic Ridge. *J. Geophys. Res.*, 89:11379–11400.

Ito, E., and Anderson, A. T., Jr., 1983. Submarine metamorphism of gabbros from the Mid-Cayman Rise: petrographic and mineral constraints on hydrothermal processes at slow-spreading ridges. *Contrib. MineraL. Petrol.*, 82:371–388.

Ito, E., and Clayton, R. N., 1983. Submarine metamorphism of gabbros from the Mid-Cayman Rise: an oxygen isotopic study. *Geochem. Cosmochim. Acta*, 47:535–546.

Ito, E., Harris, D. M., and Anderson, A. T., Jr., 1983. Alteration of oceanic crust and geologic cycling of chlorine and water. *Geochem. Cosmochim. Acta*, 47:1613–1624.

Kelley, D. S., and Delaney, J. R., 1987. Two-phase separation and fracturing in mid-ocean ridge gabbros at emperatures greater than 700°C. *Earth Planet. Sci. Lett.*, 83:53–66.

Liou, J. G., 1971. Analcime equilibria. *Lithos*, 4:389–462.

Liou, J. G., Kuniyoshi, S., and Ito, K., 1974. Experimental studies of the phase relations between greenschist and amphibolite in a basaltic system. *Am. J. Sci*, 274:613–632.

Liou, J. G., Kim, H. S., and Maruyama, S., 1983. Prehnite-epidote equilibria and their petrologic applications. *J. Petrol.*, 24:321–342.

Manning, C. E., and Bird, D. K., 1986. Hydrothermal clinopyroxenes of the Skaergaard intrustion. *Contrib. Mineral. Petrol*, 92:437–447.

Maruyama, S., Suzuki, K., and Liou, J. G., 1983. Greenschist-amphibolite transition equilibria at low pressure. *J. Petrol.*, 24:583–604.

Matthews, A., Goldsmith, J. R., and Clayton, R. N., 1983. Oxygen isotope fractionations involving pyroxenes: the calibration of mineral-pair geothermometers. *Geochim. Cosmochim. Acta*, 47:631–644.

Mevel, C., 1987. Evolution of oceanic gabbros from DSDP Leg 82: influence of the fluid phase on metamorphic crystallizations. *Earth Planet. Sci. Lett.*, 83:67–79.

_______, 1988. Metamorphism in oceanic layer 3 Gorringe Bank, Eastern Atlantic. *Contrib. Mineral. Petrol.*, 100:496–509.

Muehlenbachs, K., and Clayton, R. N., 1976. Oxygen isotopic composition of the oceanic crust and its bearing on seawater. *J. Geophys. Res.*, 81:4365–4369.

Norton, D., Taylor, H. P., Jr., and Bird, D. K., 1984. The geometry and high-temperature brittle deformation of the Skaergaard intrusion. *J. Geophys. Res.*, 89:10178–10192.

O'Neil, J. R., and Taylor, H. P., Jr., 1967. The oxygen isotope and cation exchange chemistry of feldspars. *Am. Mineral.*, 52:1414–1437.

Page, N. J., and Zientek, M. L., 1987. Composition of primary postcumulus amphibole and phlogopite within an olivine cumulate in the Stillwater Complex, Montana, U.S. Geol. Surv. Bull. 1674-A, *Contributions on Ore Deposits in the Early Magmatic Environment*: Washington (U.S. Govt. Printing Office).

Papike, J. J., Cameron, K. L., and Baldwin, K., 1974. Amphiboles and pyroxenes: characterization of other than quadrilateral components and estimates of ferric iron from microprobe data (abst.). *Geol. Soc. Am. Abst. with Prog.*, 6:1053–1054.

Plyusnina, L. P., 1982. Geothermomtry and geobarometry of plagioclase-hornblende bearing assemablages. *Contrib. Mineral. Petrol.*, 80:140–146.

Prichard, H. M., and Cann, J. R., 1982. Petrology and mineralogy of dredged gabbro from Gettysburg Bank, Eastern Atlantic. *Contrib. Mineral. Petrol.*, 79:46–55.

Robinson, P., Spear, F. S., Schumacher, J. C., Laird, J., Klein, C., Evans, B. W., and Doolan, B. L., 1982. Phase relations of metamorphic amphiboles: natural occurrence and theory. *In*: Veblen, D.R. and Ribbe, P.H. (Eds), *Amphiboles: Petrology and Experimental Phase Relations*. Rev. Mineral., 9B: Washington (Mineral. Soc. Am.).

Shipboard Scientific Party, 1989. Site 735. *In* Robinson, P. T., Von Herzen, R., *Proc. ODP, Init. Repts.*, 118: College Station, TX (Ocean Drilling Program), 89–222.

Spear, F. S., 1980. NaSi==CaAl exchange equilibrium between plagioclase and amphibole: an empirical model. *Contrib. Mineral. Petrol.*, 72:33–41.

Stakes, D. S.and O'Neil, J. R., 1982. Mineralogy and stable isotope geochemistry of hydrothermally altered oceanic rocks. *Earth Planet. Sci. Lett.*, 57:285–304.

Stakes, D. S., Taylor, H. P., Jr., and Fisher, R. L., 1983. Oxygen-isotope and geochemical characterization of hydrothermal alteration in ophiolite complexes and modern oceanic crust. *In* Gass, I. G., Lippard, S. J., and Shelton, A. W.(Eds.) *Ophiolites and Oceanic Lithosphere*: London (Blackwell), 199–204.

Stakes, D. S., and Vanko, D. A., 1986. Multistage hydrothermal alteration of gabbroic rocks from the failed Mathematician Ridge. *Earth Planet. Sci. Lett.*, 79:75–92.

Strens, M. R., and Cann, J. R., 1982. A model of hydrothermal circulation in fault zones at mid-ocean ridge crests, Geophys. *J. Royal Astron. Soc.*, 71:225–240.

Taylor, H. P., Jr., 1968. The oxygen isotope geochemistry of igneous rocks. *Contrib. Mineral. Petrol.*, 19:1–17.

_______, 1977. Water/rock interactions and the origin of H_2O in granitic batholiths. *J. Geol. Soc.* (*London*), 133:509–558.

_______, 1984. Oxygen and hydrogen isotope studies of hydrothermal interactions at submarine and subaerial spreading centers, *In* Rona, P. A., Bostrom, K., Laubier, L., and Smith, K. (Eds.), *Hydrothermal Processes at Seafloor Spreading Centers*, NATO Marine Science Ser. IV, Vol. 12: New York (Plenum Press).

Vanko, D. A., and Batiza, R., 1982. Gabbroic rocks from the Mathematician Ridge failed rift. *Nature*, 300:742–744.

Date of initial receipt: 18 August 1989
Date of acceptance: 26 June 1990
Ms 118B-127

APPENDIX

Detailed Descriptions of Type Thin Sections and Microprobe Analyses

Examples of each type of metamorphism are provided with detailed phase assemblage information, as follows:

1. High-temperature, low-water/rock deformation assemblage: (1) Sample 118-735-85-4, (Pc. 1c, 17–25 cm). This is a foliated gneissic gabbro from the lower shear zone cut by hornblende veins. It texturally resembles deformed rocks from the shallower deformed zones. There are large clinopyroxene augen that are compositionally similar to igneous clinopyroxene. Some of the clinopyroxene grains show numerous narrow multiple twins, likely resulting from deformation (S. Kirby, pers. comm., 1989). Neoblasts of clinopyroxene, hornblende, and possible orthopyroxene surround the porphyroclasts. The clinopyroxene neoblasts are slightly more diopsidic than

the adjacent porphyroclasts. Deeply colored brown and green aluminous hornblende can be seen both as a synkinematic phase and as filling the crosscutting veins. Amphibole compositions are provided in Table 4. Plagioclase neoblasts are $An_{51\text{-}54}$, whereas secondary plagioclase intergrown with the green hornblende is more sodic, $An_{18\text{-}16}$. A late vein of epidote (Ps_{17}) crosscuts the plagioclase mosaic. Deformed apatite grains and brown hornblende were found not to contain chlorine. (2) Sample 118-735-14R-3, (Pc. 2A, 31–35 cm). This foliated metagabbro originally contained olivine that is now statically (post-deformation) replaced by cummingtonite and phlogopite, or by a low-temperature assemblage of carbonate and hematite. Lenses of chlorite replace plagioclase. Plagioclase porphyroclasts and neoblasts are homogeneous in composition, An_{48}. Clinopyroxene neoblasts are slightly more diopsidic than pyroxene porphyroclasts. Amphibole compositions are similar in vein fillings and foliation planes (Vanko and Stakes, this volume).

2. High to moderate-temperature high-water/rock deformation assemblage: (1)Sample 118-735-1D-1 (Pc. 4, 26–30 cm): This porphyroclastic to mylonitic gabbro has synkinematic hornblende observed in the pressure shadows adjacent to clinopyroxene porphyroclasts. Pale brown aluminous hornblende is associated with large plagioclase neoblasts (An_{41}) and bands of ilmenite. The bright green actinolitic hornblende is intergrown with sodic plagioclase (An_{21}) in the finer-grained mosaic. There is no diopside, chlorite, or epidote, although some phlogopite was observed in discontinuous tension cracks in the plagioclase. Actinolite pseudomorphs clinopyroxene porphyroclasts and pale tremolite pseudomorphs olivine. A late oxidative overprint is evidenced by abundant red Fe-oxide, brown smectite, celadonite, and traces of carbonate.

3. Moderate-temperature, high-water/rock deformation assemblage: (1) Sample 118-735B-58R-2, (Pc. 1B, 10–17 cm). A thin mylonite zone crosscuts a metagabbro (Pl. 2, Fig. 3) with extensive alteration of the host gabbro. Synkinematic hornblende was found in the tails of clinopyroxene porphyroclasts as well as in the mylonite zones. The cores of the clasts are actinolitic hornblende. See Table 6 for amphibole compositions. The fine-grained material in the mylonite bands is albite and fibrous actinolitic hornblende, with rounded neoblasts of actinolitic hornblende. Metamorphic plagioclase (large polygonal neoblasts) adjacent to the mylonite band is An_{28}, and the contemporaneous green bladed amphibole is magnesio-hornblende. Most of the undeformed plagioclase in the host has retained an igneous composition of $An_{52\text{-}57}$, although small grains of An_{40} were observed. Olivine has been replaced by tremolite and magnetite, while the olivine-plagioclase grain boundaries have been replaced by actinolitic hornblende (see Table 6 and Vanko and Stakes, this volume for typical amphibole compositions). Clinopyroxene has retained a normal igneous composition because it has not recrystallized under these conditions (Table 3). Phase compositions for an olivine-rich foliated metagabbro (Sample 118-735B-8D-1, Pc. 4) are provided in Tables 2 through 4 and 9. In this example, it is clear that the recrystallized olivine is identical in composition to the olivine porphyroclasts. The amphibole compositions are also distinctive: synkinematic hornblende is rich in Ti and contains no Cl, while vein hornblende is low in Ti and rich in Cl.

4. Hornblende (-plagioclase) veins: (1) Sample 118-735B-20R-2 (Pc. 1E, 10–13 cm). A 2- to 3-cm-wide plagioclase-hornblende vein crosscuts a pervasively amphibolitized gabbro. The plagioclase composition varies from An_{18} to An_{32}, while the most sodic compositions are intergrown with rare grains of clinozoisite (Table 8) in the vein. The hornblende is deep green and contains up to 12% Al_2O_3. Euhedral plagioclase (both within and adjacent to the vein) has a peculiar mottled extinction, which proved to be intergrown An_{26} and An_{32} compositions. This texture has been interpreted as a replacement of primary plagioclase by sodic plagioclase. The complete pseudomorphous replacement of the host rock adjacent to the vein results in the "vein assemblage" occupying much more space than the original crack through which fluid moved. There are apparently minor variations in secondary mineral compositions between those that formed in the vein compared with those that replaced the host. (2) Sample 118-735B-22R-4 (Pc. 1A, 0–3 cm). This extensively veined gabbro contains relict calcic plagioclase (An_{59}) that has been cut by anastomosing veins of sodic plagioclase (An_{20}) and clinopyroxene that has been almost completely replaced by actinolitic hornblende. The same phases appear intergrown in crosscutting veins—actinolitic hornblende is associated with sodic plagioclase ($A_{26\text{-}30}$). The plagioclase porphyroclasts and mantles of brown hornblende on the pseudomorphed clinopyroxene suggest limited early ductile deformation. In addition, in Samples 118-735-19R-2, Pc. 12, 98–100 cm) and 118-735-22R-1, Pc. 17, 142–147 cm, a similar, pervasively altered gabbro has been crosscut by analcime veins (Table 8) with actinolite fibers as well as chlorite. Both of these phases are inferred to be a replacement of the sodic plagioclase under lower temperatures. Epidote appears in a sheared vein in Sample 118-735-30R-2, Pc. 13D, 120–122 cm, associated with sodic plagioclase and containing actinolite fibers.

5. Coronitic replacements: (1) Sample 118-735B-35R-7 (Pc. 2, 14–17 cm). See Tables 6 and 7 for examples of phase compositions. This is an olivine gabbro from within the shallowest zone crosscut by hydrothermal veins. Olivine ($Fo_{62\text{-}65}$; Table 9) crystals have been replaced by coronas of talc, cummingtonite and magnetite. Olivine-plagioclase ($An_{41\text{-}44}$) grain boundaries were replaced by intergrown phlogopite and pargasitic hornblende and by pale chlorite. Ferroan pargasitic hornblende veins crosscut the core at very steep angles. Relict clinopyroxene has been replaced either by diopside or by actinolite. Diopsidic neoblasts are intergrown with edenitic hornblende. (2) Sample 118-735B-82-7 (Pc. 2, 21–29 cm). This is an undeformed olivine gabbro having coronitic alteration. Edenitic hornblende has filled cracks and replaced calcic plagioclase ($An_{60\text{-}62}$). Olivine (Fo_{75}; Table 7) has been replaced by tremolite. Olivine-plagioclase grain boundaries have been replaced by radial aggregates of actinolitic hornblende, very large flakes of phlogopite, and pale chlorite. Magnesio-hornblende and actinolitic hornblende have replaced the igneous augite. (3) Sample 118-735B-78R-3 (Pc. 5, 62–64 cm). This heavily veined and altered gabbro suggests a combination of hydrous replacement and hydrothermal mineralization. Sodic plagioclase ($An_{17\text{-}22}$) formed rims on calcic plagioclase (An_{67}) and neoblasts ($An_{58\text{-}65}$). Primary brown tschermakitic hornblende is found as interstitial rims on and blebs within pyroxene. Primary red biotite grains are euhedral, while secondary green to brown phlogopite appears in coronitic replacement of olivine. Cummingtonite has replaced olivine and orthopyroxene lamellae in clinopyroxene. Talc and magnetite are also present in the olivine pseudomorphs. Sphene replaced ilmenite. Traces of epidote have replaced plagioclase.

6. LMI and evidence for assimilation: (1) Sample 118-735B-7D-1 (Pc. 2A, 10–16 cm): Small volumes of zircon-bearing felsic pegmatoidal gabbro containing large euhedral plagioclase (An_{30}) from Sample 118-735B-7D-1, Pc. 2A (10–16 cm) provided the lead isotope age of the core. This LMI (or ferrogabbro) was in contact with an isoclinally folded porphyroclastic olivine gabbro with more calcic porphyroclasts (An_{47}) and neoblasts ($An_{43\text{-}46}$). The large zircon grains were broken, suggesting limited deformation, in contrast to the adjacent highly deformed gabbro. Apparently, the olivine gabbro was deformed, the zircon pegmatite was intruded, and then a second deformation occurred. (2) Sample 118-735B-53R-4 (Pc. 1B, 5–15 cm). Sections 118-735B-53R-3 to -53R-4 are Fe-Ti oxide-rich gabbros crosscut by late felsic intrusions. In this sample, a vein of LMI crosscuts a foliated gabbro, illustrating that LMI must have been present during post-ductile deformation. The center of the LMI vein is sodic plagioclase ($An_{16\text{-}18}$) fringed with apatite, small skeletal diopside grains, cummingtonite, and zircon (Pl. 1, Fig. 2). The margins on the plagioclase are rich in dark inclusions, a common feature of the LMI. This may result from a subsolidus exsolution of excess Fe as magnetite in the rims of the sodic plagioclase. Bundles of cummingtonite are mixed with grains of magnetite and are inferred to be pseudomorphs of pyroxene. Large plagioclase grains and neoblasts in the host gabbro are $An_{32\text{-}29}$, with a few grains showing strong zonation to rims of An_{20} (Table 5). Pyroxene in the host gabbro (Tables 2, 3, 4, and Fig. 3) is jacketed by brown, synkinematic magnesio-hornblende (see Table 5, Vanko and Stakes, this volume), while the cores have been replaced by ferro-actinolite. (3) Sample 118-735B-73R-6 (Pc. 1B, 8–10 cm) is an example of the late magmatic liquid with small, dark, partially digested xenoliths. Section 118-735B-73R-6 has been injected by a plagioclase-hornblende vein having sparse corroded diopside grains. Mineral compositions are provided in Tables 2 through 6 and Vanko and Stakes (this volume). The center of the intruding "vein" is composed of euhedral, blocky, twinned igneous plagioclase that is An_{24} in composition (Pl. 1, Fig. 1). The core of a large plagioclase xenocrysts was found to be $An_{40\text{-}42}$, with margins decorated with

euhedral secondary grains that are An_{24-31} in composition. The twinned euhedral grains in the adjacent LMI are An_{35}. Corroded relicts of diopside contain up to 0.6% Al_2O_3. A few large relict clinopyroxenes contain up to 1.5% Al_2O_3, and clinopyroxene neoblasts are intermediate in composition. It is not clear if this is a result of interaction with the LMI; however, the limited variability of pyroxene compositions from all three occurrences (Figs. 3A,and 3B) certainly suggests this. We infer from these mineral compositions and textural relationships that the gabbro xenoliths have been partially digested by the LMI, producing sodic plagioclase and diopsidic pyroxene or brown hornblende.

Brown Ti-rich actinolitic hornblende having euhedral inclusions of sodic plagioclase (An_{25}) rims clinopyroxene xenocrysts. Where tiny cracks cross the large pyroxenes, green magnesio- or tschermakitic-hornblende was observed as a replacement phase. Neither the aluminous hornblende nor the fibrous actinolitic hornblende contain chlorine. In much of the vein, hornblende is the only mafic phase associated with sodic plagioclase. This presumably reflects a more hydrous fluid phase that produced the secondary diopside. Sample 118-735B-78R-3 (Pc. 5D, 110–119 cm) is an undeformed gabbro that has been crosscut by a plagioclase-aluminous hornblende vein, similar to the phases observed in the previous sample. We infer that some of the hydrous fluids derived from the zones of LMI injections could play a role in forming these veins in the adjacent gabbro. Infiltration: (4) Sample 118-735B-35R-2 (Pc. 4G, 105–108 cm); see Vanko and Stakes (this volume) for phase compositions. This coarse-to medium-grain gabbro has a mesocumulate texture and has been cut by a 1-cm-wide deformation zone (Shipboard Scientific Party, 1989). Within this deformation zone is a fine-grained LMI with an assemblage that includes sodic plagioclase (An_5, An_{16}), quartz, actinolite, diopside, zircon, biotite (Table 5), sulfide, and apatite. The host rock and sections of core up to 5 m from this zone contain metamorphic phlogopite as part of the reaction coronas around olivine. The host gabbro has been pervasively altered, with relict clinopyroxene replaced by diopside and actinolitic hornblende (Table 4), and calcic plagioclase replaced by sodic plagioclase (An_{31-23}).

7. Cataclastic assemblage: (1) Sample 118-735B-45R-4 (Pc. 7, 136–140 cm): This gabbro is slightly deformed with synkinematic pargasitic hornblende and ilmenite and has been pervasively replaced by hydrothermal minerals. Vein minerals include analcime, edenitic hornblende, and traces of carbonate. Abundant epidote ($Ps_{15,19}$), anastomosing analcime veinlets, and radial chlorite aggregates have replaced calcic plagioclase (An_{63}). The chlorite is more Fe-rich than that observed in the coronitic replacements. No sodic plagioclase was found during our microprobe analyses. Hydrothermal apatite is large, Cl-bearing, and contains abundant fluid inclusions (see Vanko and Stakes, this volume). Late actinolite has been intergrown with the earlier, synkinematic pargasite and is presumably its replacement. Large pink sphene is intergrown with ilmenite in a trellis texture, and was similarly inferred to be a replacement texture. Ilmenite, pyrite, and chlorite were also observed intergrown in a trellis texture. These "trellis" textures are inferred to be inherited from a subsolidus exsolution of two phases along crystallographic planes. Diopside-sphene intergrowths have replaced clinopyroxene (Tables 2 through 4 and Fig. 3B). Olivine has been almost completely replaced by anthophyllite and talc. (2) Sample 118-735B-57R-2 (Pc. 1B, 11–18 cm) is a felsic gabbro breccia adjacent to a major autoclastic gabbro breccia zone. This brecciated gabbro has an extraordinarily heterogeneous texture. Plagioclase (An_{32-24}) has broad jackets of secondary sodic plagioclase (An_{16-21}) (Pl. 2, Fig. 6) and intergrown brown magnesio-hornblende and sodic plagioclase (An_{24-18}) rim clinopyroxene (Pl. 2, Fig. 5). Small euhedral grains of plagioclase (An_{10}-An_{24}) resemble the ones crystallized from the LMI. Radial plates of analcime, aggregates of chlorite (Table 7), and dark patches of smectite are evidence of lower temperature replacements. Amphibole is strongly zoned (Pl. 1, Fig. 3) and compositionally varies from an actinolitic hornblende core to a magnesio-hornblende to rims of ferroactinolite.

8. Diopside-bearing veins: (1) Sample 118-735B-64R-4 (Pc. 1H, 73–76 cm): This hydrothermal vein crosscuts an unfoliated, extensively amphibolitized olivine gabbro. Phase compositions are provided in Tables 2 through 4. This vein is near an unsealed fracture with carbonate on one surface, suggesting access of cold seawater after the cessation of hydrothermal activity. This vein is massive and over 2 cm thick. Primary plagioclase (An_{67-62}) of the host is altered to more sodic compositions (An_{41-44}). Vein plagioclase is An_{20-27} and is contemporaneous with diopside that is strongly zoned in Fe-content (Fig. 3B). More magnesian diopsides replace igneous pyroxene. Vein plagioclase is partially replaced by chlorite and epidote (Pcs. 11, 15; Table 8). There is no hornblende present in the vein, although actinolite replaces some of the plagioclase and igneous clinopyroxene. (2) Sample 118-735B-66R-4 (Pc. 4, 14–19 cm). This is a sample from what was described as a hydrothermally deformed gabbro, with limited foliation and pervasive brecciation (Shipboard Scientific Party, 1989). Primary calcic plagioclase (An_{64-58}) is crushed (An_{40-52}) and crosscut by veins of sodic plagioclase (An_{34-15}) and diopside (Fig. 3B and Tables 2 through 6). Small euhedral grains of sodic plagioclase show some zonation (e.g., An_{21-17}). Diopside compositions also vary in Fe-content. Actinolitic hornblende has formed a fringe on many of the diopside grains, and is inferred to be replacing the pyroxene. Pale actinolite has replaced patches of the crushed plagioclase, and some relict (?) grains of synkinematic magnesio-hornblende are also present. (3) Sample 118-735B-65R-2 (Pc. 1B, 18–25 cm). A diopside vein crosscuts large altered plagioclase and clinopyroxene grains. Laths of pargasitic hornblende (Table 5, Vanko and Stakes this volume) replaced the plagioclase, while the igneous clinopyroxene was replaced by diopside, actinolite, and hornblende. Figure 3B depicts the compositions of the vein diopside, as well as a traverse from the vein into the adjacent clinopyroxene grain. This vein is pure diopside, while the replacement diopside is more enstatite-rich. A parallel traverse through the adjacent plagioclase reveals compositions of An_{55-59} farthest from the vein, more calcic plagioclase near the vein (An_{65-66}), and plagioclase of variable composition adjacent to the diopside (An_{30-53}). This change in the composition of plagioclase occurred over a distance of 7 mm in a single grain of plagioclase. We suggest that Fe-poor diopside and sodic plagioclase have been replacing the plagioclase within a few millimeters of the vein. Diopside found either as an apparent replacement of plagioclase or as euhedral grains in the veins are extremely calcic with variable Fe concentrations. Diopside that replaces the igneous augite is less calcic and more magnesian. These chemical variations are clearly related to fluids penetrating along cracks and shears and are not igneous.

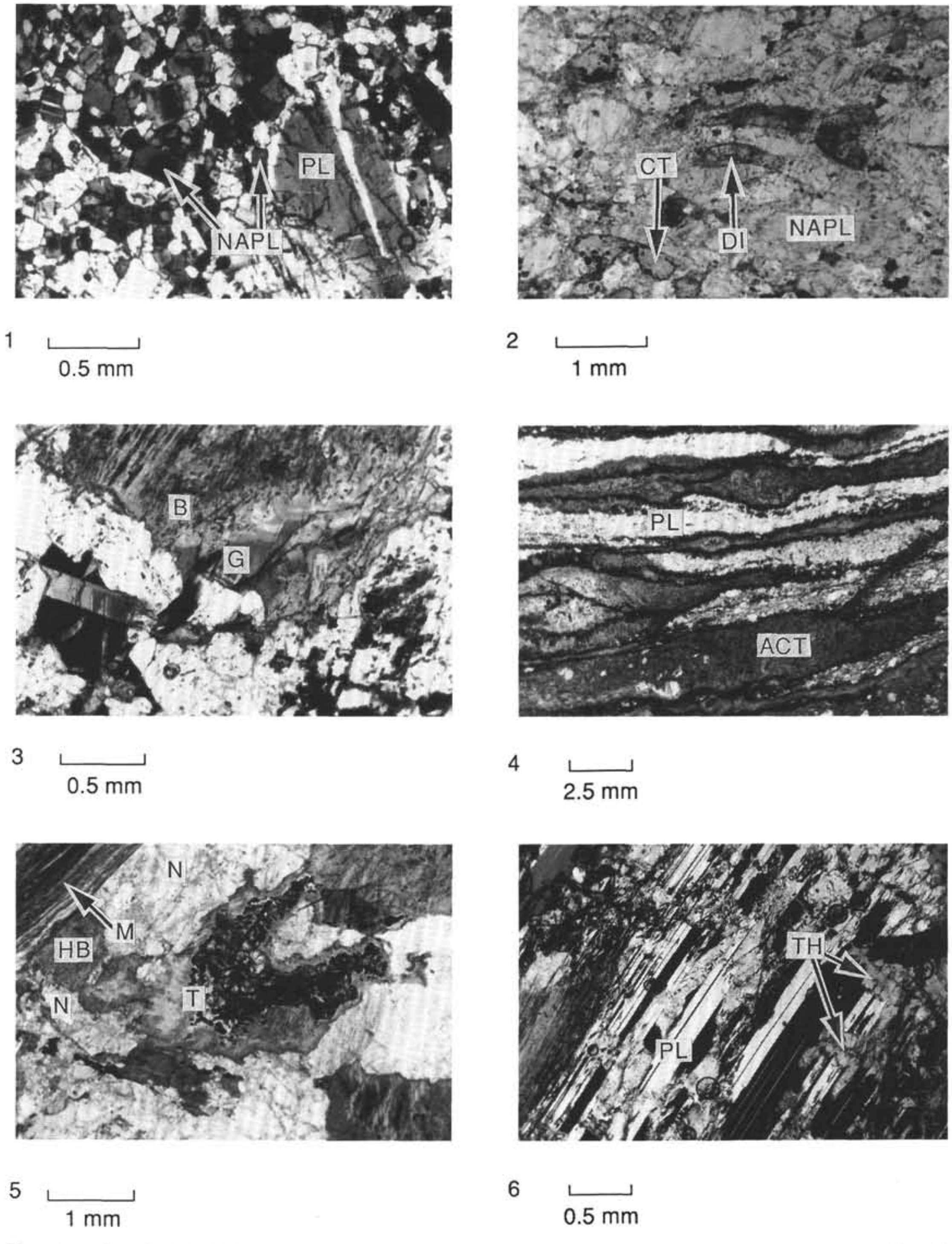

Plate 1. **1.** Sample 118-735-73R-6, Pc.1B. Photomicrograph of late magmatic liquid surrounding xenocrysts of calcic plagioclase ($AN_{40\text{-}42}$; PL). Phases in LML include sodic plagioclase ($AN_{35\text{-}24}$), diopside, zircon, actinolitic hornblende. Note recrystallization of plagioclase xenocryst into small euhedral sodic plagioclase along margin (NAPL). This is inferred to result from assimilation. (crossed nicols). **2.** Sample 118-735-53R-4, Pc. Photomicrograph of a vein of late magmatic liquid, containing zircon, diopside (DI) , sodic plagioclase (NAPL; $AN_{16\text{-}18}$), and bundles of cummingtonite (CT) and magnetite (plane light). **3.** Sample 118-735-57R-2, Pc. 1. Photomicrograph of secondary minerals in hydrothermal breccia. Primary clinopyroxene has rim of brown hornblende (B) that grades into strongly zoned green hornblende (G) in open fractures that varies in composition (core to rim) from actinolitic hornblende to magnesio-hornblende to ferro-actinolite. This texture is inferred to represent episodic mineral growth within an open crack (plane light). **4.** Sample 118-735-7D-1, Pc. 15. Photomicrograph of a gneiss that has been statically altered to a mixture of fibrous actinolite (ACT) and sodic plagioclase (PLG) (plane light). **5.** Sample 118-735-58R-2, Pc. 1B. Photomicrograph of thin mylonite zone (M) cutting gabbro and associated coronitic replacement of igneous phases. Mylonite (dark band in upper left corner) is compossed of fine-grained albite and fibrous actinolitic hornblende. Adjacent polygonal neoblasts (N) are plagioclase (AN_{28}) and bladed magnesio-hornblende (HB). Olivine is replaced by tremolite (T) and magnetite (plane light). **6.** Sample 118-735-63R-5, Pc. 4A. Photomicrograph of anastomozing veins of thomsonite (TH) replacing plagioclase (PL) (crossed nicols).

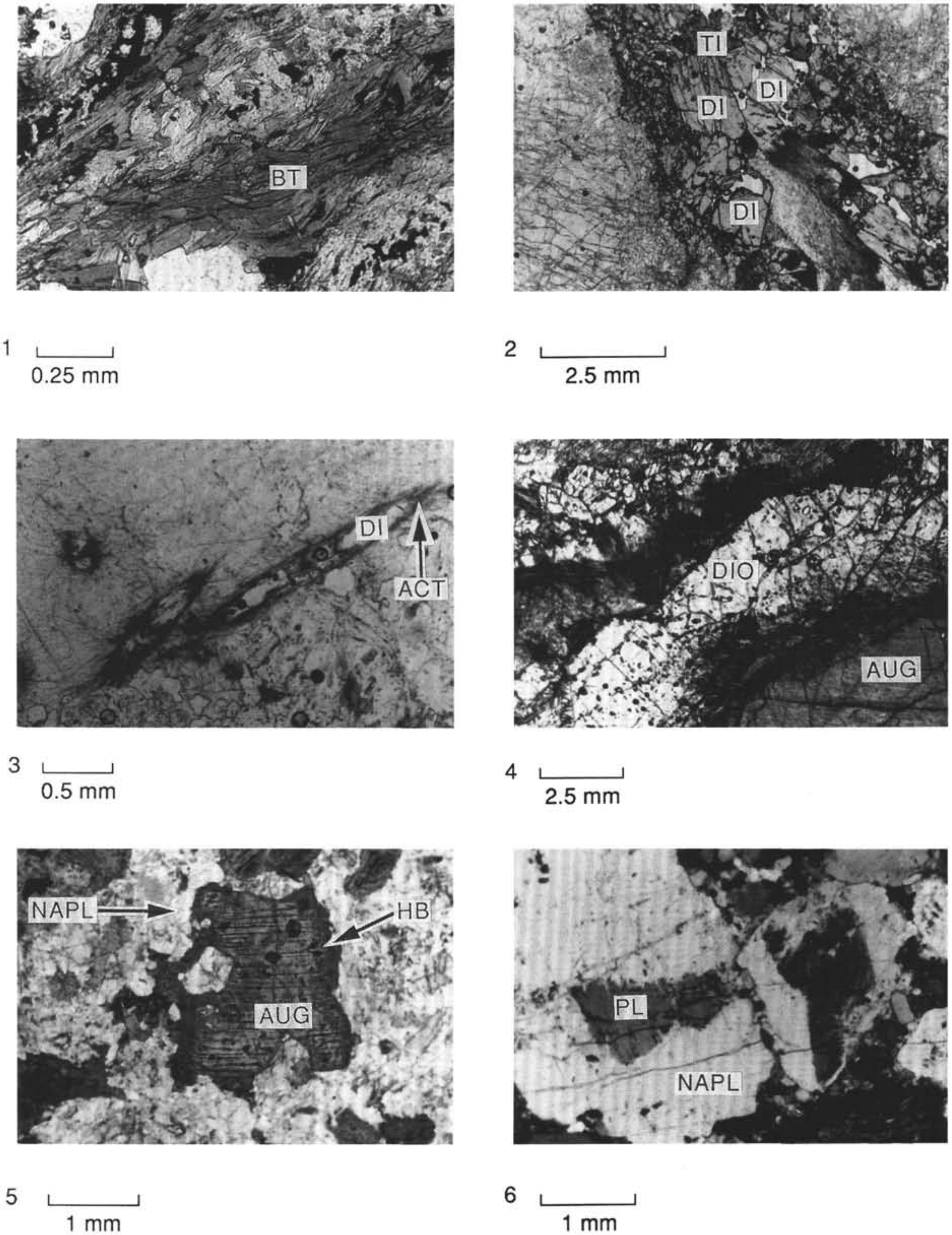

Plate 2. **1.** Sample 118-735-2D-1, Pc. 12. Photomicrograph of synkinematic green biotite (BT). Small flakes are oriented parallel to foliation with neoblasts of brown hornblende (plane light). **2.** Sample 118-735-77R-4, Pc. 13. Photomicrograph of hydrothermal vein with clinopyroxene (DI), sphene (TI), and thomsonite (X1, plane light). **3.** Sample 118-735R-63R-6, Pc. 5B. Photomicrograph of secondary diopside in vein fringed with fibrous actinolite (X4, plane light). **4.** Sample 118-735-64R-1, Pc. 4B. Photomicrograph showing aureole of secondary diopside (DIO) replacing primary igneous clinopyroxene (AUG) (plane light). **5.** Sample 118-735-57R-2, Pc. 1B. Photomicrograph of igneous clinopyroxene (AUG) mantled with brown hornblende (HB) and sodic plagioclase (NAPL) (plane light). **6.** Sample 118-735-57R-2, Pc. 1B. Photomicrograph of igneous plagioclase (PL) with broad jacket of sodic plagioclase (NAPL) (crossed nicols).